

RESEARCH ARTICLE

10.1029/2018JG004484

Key Points:

- The use of a C₃/C₄ fraction map derived from Cropland Data Layer (CDL) improves gross primary production (GPP) estimates over croplands
- GPP estimates by Vegetation Photosynthesis Model are highly correlated with solar-induced chlorophyll fluorescence (SIF)
- Increased GPP in the warm spring offsets the reduced GPP by summer drought in 2012 over CONUS

Correspondence to:

X. Xiao,
xiangming.xiao@ou.edu

Citation:

Wu, X., Xiao, X., Zhang, Y., He, W., Wolf, S., Chen, J., et al. (2018). Spatiotemporal consistency of four gross primary production products and solar-induced chlorophyll fluorescence in response to climate extremes across CONUS in 2012. *Journal of Geophysical Research: Biogeosciences*, 123, 3140–3161. <https://doi.org/10.1029/2018JG004484>

Received 9 MAR 2018

Accepted 10 SEP 2018

Accepted article online 15 SEP 2018

Published online 8 OCT 2018

Spatiotemporal Consistency of Four Gross Primary Production Products and Solar-Induced Chlorophyll Fluorescence in Response to Climate Extremes Across CONUS in 2012

Xiaocui Wu¹ , Xiangming Xiao^{1,2} , Yao Zhang¹ , Wei He^{3,4} , Sebastian Wolf⁵ , Jiquan Chen⁶ , Mingzhu He⁷, Christopher M. Gough⁸ , Yuanwei Qin¹ , Yanlian Zhou⁹, Russell Doughty¹ , and Peter D. Blanken¹⁰ 

¹Department of Microbiology and Plant Biology, Center for Spatial Analysis, University of Oklahoma, Norman, OK, USA, ²Ministry of Education Key Laboratory of Biodiversity Science and Ecological Engineering, Institute of Biodiversity Science, Fudan University, Shanghai, China, ³International Institute for Earth System Science, Nanjing University, Nanjing, China, ⁴Center for Isotope Research (CIO), Energy and Sustainability Research Institute Groningen (ESRIG), University of Groningen, Groningen, The Netherlands, ⁵Department of Environmental Systems Science, ETH Zurich, Zurich, Switzerland, ⁶Center for Global Change and Earth Observations (CGCEO), Michigan State University, East Lansing, MI, USA, ⁷Numerical Terradynamic Simulation Group, College of Forestry and Conservation, University of Montana, Missoula, MT, USA, ⁸Department of Biology, Virginia Commonwealth University, Richmond, VA, USA, ⁹Jiangsu Provincial Key Laboratory of Geographic Information Science and Technology, School of Geographic and Oceanographic Sciences, Nanjing University, Nanjing, China, ¹⁰Department of Geography, University of Colorado Boulder, Boulder, CO, USA

Abstract Large spatial-scale effects of climate extremes on gross primary production (GPP), the largest terrestrial carbon flux, are highly uncertain even as these extremes increase in frequency and extent. Here we report the impacts of spring warming and summer drought in 2012 on GPP across the contiguous United States (CONUS) using estimates from four GPP models: Vegetation Photosynthesis Model (VPM), MOD17A2H V006, Carnegie-Ames-Stanford Approach, and Simple Biosphere/Carnegie-Ames-Stanford Approach. VPM simulations are driven by Moderate Resolution Imaging Spectroradiometer, North American Regional Reanalysis climate data, and C₃ and C₄ cropland maps from the United States Department of Agriculture Cropland Data Layer data set. Across 25 eddy covariance flux tower sites, GPP estimates from VPM (GPP_{VPM}) showed better accuracy in terms of cross-site variability and interannual variability ($R^2 = 0.84$ and 0.46, respectively) when compared to MOD17 GPP. We further assessed the spatial and temporal (seasonal) consistency between GPP products and the Global Ozone Monitoring Experiment-2 solar-induced chlorophyll fluorescence over CONUS during 2008–2014. The results suggested that GPP_{VPM} agrees best with solar-induced chlorophyll fluorescence across space and time, capturing seasonal dynamics and interannual variations. Anomaly analyses showed that increased GPP during the spring compensated for the reduced GPP during the summer, resulting in near-neutral changes in annual GPP for the CONUS. This study demonstrates the importance of assessing the impacts of different types and timing of climate extremes on GPP and the need to improve light use efficiency models by incorporating C₃ and C₄ plant functional types.

1. Introduction

Terrestrial ecosystems play a major role in the global carbon cycle, offsetting approximately 25–30% of the CO₂ emitted by human activities since the 1950s (Le Quéré et al., 2009). Gross primary production (GPP), the amount of CO₂ sequestered by vegetation through photosynthetic assimilation before accounting for respiratory losses, is the largest component of the global terrestrial carbon flux (Beer et al., 2010). Therefore, a small fluctuation in GPP could have significant impact on atmospheric CO₂ concentrations. However, the composition, structure, and functioning of terrestrial ecosystems are expected to be substantially altered by increases in the duration or/and frequency of climate extremes such as droughts, heatwaves, or intense precipitation events (Frank et al., 2015). It is a major challenge to understand and project the response of terrestrial ecosystems to climate extremes (Reichstein et al., 2013). In particular, droughts, together with the frequently co-occurring heatwaves, are among the most widespread natural disasters and could have large impacts on annual GPP, ecosystem respiration (ER), and net carbon balance (Frank et al., 2015; van der Molen et al., 2011).

The impacts of climate extremes, especially heatwaves and droughts, on GPP have been thoroughly investigated for selected events (Ciais et al., 2005; Parazoo et al., 2015; Wolf et al., 2016; Yuan et al., 2016). However, how climate extremes affect the carbon cycle is still poorly known at the landscape, regional, and global scales (Pan & Schimel, 2016). To investigate the impacts of climate extremes on GPP at ecosystem and landscape scales, three approaches have been separately or jointly applied: eddy covariance (EC) flux tower measurements (von Buttlar et al., 2017; Welp et al., 2007), remote sensing data (Hilker et al., 2014), and biogeochemical models (Zscheischler et al., 2014). Since the 1990s, the EC flux tower method has provided directly observed evidence for the seasonal changes of terrestrial carbon fluxes, which increases our understanding of the underlying mechanisms of terrestrial ecosystem responses and their feedbacks to climate extremes at the site scale (Reichstein et al., 2007). However, in situ EC sites are limited by their relatively moderate-size footprints of observation and the number and distribution of FLUXNET sites are limited, making it difficult to assess the impacts of climate extremes on the carbon cycle at regional, continental, and global scales. The GPP data derived from EC flux towers (GPP_{EC}), though limited in their spatial coverage, are currently the best available data to validate GPP estimates from process-based and data-driven GPP models. In contrast, optical and microwave remote sensing data provide larger scale insights into the vegetation structure, including leaf area index and light absorption by canopy (J. M. Chen, 1996; Disney et al., 2006; Ollinger, 2011). Recently, solar-induced chlorophyll fluorescence (SIF) data have been derived from satellite-based observations to estimate GPP, as it is tightly linked with photosynthesis (Frankenberg et al., 2011; Porcar-Castell et al., 2014). However, SIF has a very weak signal and accounts for about 2% of the total light absorbed by vegetation. Satellite-retrieved SIF measurements have comparatively large amounts of noise, and the recent SIF data products are often aggregated in temporal and spatial domains resulting in a coarse spatial and temporal resolution (monthly, $0.5^\circ \times 0.5^\circ$ for Global Ozone Monitoring Experiment-2, GOME-2; Joiner et al., 2013). The coarse spatial resolution of SIF data products limits its application because 0.5° gridcells (~ 50 km at Equator) are often highly heterogeneous. A final approach uses terrestrial biosphere models to estimate GPP and ER for a variety of ecosystems at multiple scales. However, the reliability of these models is constrained by input data sets, model parameters, and model structures (Schaefer et al., 2012; Schwalm et al., 2010). Hence, a synthesis and comparison of the different approaches can reveal the shortcomings of individual approaches and help to reach a more reliable assessment of the multiple-scale responses of ecosystems to climate extremes (Pan & Schimel, 2016).

In 2012, the Contiguous United States (CONUS) experienced an abnormally warm spring and dry summer (Hoerling et al., 2014; Knutson et al., 2013). Record-breaking temperatures were observed across 34 states during spring and a severe summer drought followed, especially across the Great Plains and the Midwest Corn Belt. The 2012 U.S. drought was reported as one of the worst droughts since 1988 and had a comparable magnitude and spatial extent of those during the 1930s and 1950s (Hoerling et al., 2014; Rippey, 2015). Impacts of this spring warming and summer droughts on terrestrial carbon fluxes in CONUS have been investigated, using the data from EC flux tower sites, GPP from the MOD17 data product, and net ecosystem production (NEP) from CarbonTracker (CTE2014 and CTE2015; Wolf et al., 2016). They found that the losses of NEP in the summer were offset by an unusually large increase of NEP in spring, resulting in a small gain of annual NEP over CONUS (0.11 pg C). They also reported that the decrease in GPP during summer was much larger than the increase of spring GPP, resulting in a moderate loss of annual GPP (-0.38 pg C) over CONUS in 2012. However, there are large uncertainties among the various GPP products (Schaefer et al., 2012); for example, the MOD17 GPP product has large uncertainties in croplands (Turner et al., 2006; Xin et al., 2015). Therefore, there is a need to evaluate various GPP models and their GPP data products, which will help us to better understand and assess GPP responses to spring warming and summer drought in 2012.

In this study, we analyzed GPP data products from four GPP models: (1) the Vegetation Photosynthesis Model (VPM; Xiao, Hollinger, et al., 2004; Xiao, Zhang, et al., 2004), which has been well validated at both site (Dong et al., 2015; Doughty et al., 2018; Jin et al., 2013; Wagle et al., 2015) and regional scales (Zhang, Xiao, Jin, et al., 2016; Zhang et al., 2017) in previous studies. In this study, we modified the model for cropland by separating C_3 and C_4 crops with detailed Cropland Data Layer (CDL) data; (2) MOD17 (Running et al., 2004), which is also used to evaluate the 2012 spring warming and summer drought impact on GPP in Wolf et al. (2016); (3) Simple Biosphere/Carnegie-Ames-Stanford Approach (SiBCASA)-GFED4 (van der Velde et al., 2014), and (4) CASA-GFED3 (van der Werf et al., 2006, 2010). SiBCASA-GFED4 and CASA-GFED3 models are biosphere models used in CarbonTracker Europe (CTE2014; van der Laan-Luijckx et al., 2017) and CarbonTracker (CT2014;

Peters et al., 2007), respectively, which provided the prior biosphere carbon fluxes (NEP, GPP-Respiration) in the two carbon tracker systems. We evaluated the GPP estimations from the four data sets with in situ GPP data from EC flux tower sites and SIF data from GOME-2. The objectives of this study are threefold: (1) to demonstrate the potential of differentiating C₃ and C₄ croplands for improving GPP estimates (using VPM as an example) and validate the GPP estimates against FLUXNET data; (2) to quantify and understand the spatial-temporal consistency of GOME-2 SIF data and GPP estimates from various models; and (3) to assess the impacts of spring warming and summer drought on GPP at the pixel, biome, and continental scales.

2. Materials and Methods

2.1. VPM

We used the VPM model (Xiao, Hollinger, et al., 2004; Xiao, Zhang, et al., 2004) to estimate GPP from 2008 to 2014 over CONUS. We followed the original model framework but further differentiated between C₃ and C₄ croplands, since C₃ and C₄ crops have different maximum light use efficiencies (ϵ_{\max}). The National Agricultural Statistics Service (NASS) CDLs from the United States Department of Agriculture (USDA) were used to calculate the area percentages of C₃ and C₄ croplands within each 500 m pixel over individual years (Boryan et al., 2011). According to the USDA report, the major C₄ crop-types included corn, sorghum, sugarcane, and millet, and other crop-types were considered as C₃ croplands. The GPP of each pixel was estimated by area-weighted averaged GPP (equation (1)), which was derived from area fraction maps of C₃ and C₄ croplands and MCD12Q1 land use data sets:

$$\text{GPP} = [(\text{fC}_3 \times \epsilon_{\max\text{-C}_3} \times \text{fC}_4 \times \epsilon_{\max\text{-C}_4}) \times T_{\text{scalar}} \times W_{\text{scalar}}] \times \text{APAR}_{\text{chl}}, \quad (1)$$

where fC_3 and fC_4 were the area fraction of C₃ and C₄ crops inside each cropland pixel, respectively. APAR_{chl} is photosynthetic active radiation (PAR) absorbed by chlorophyll in the canopy and is estimated from enhanced vegetation index (EVI; Huete et al., 1997) as following:

$$\text{APAR}_{\text{chl}} = 1.25 \times (\text{EVI} - 0.1). \quad (2)$$

This equation was modified from the previous model version (Xiao, Hollinger, et al., 2004; Xiao, Zhang, et al., 2004) and has been applied in generating a global GPP product (Zhang et al., 2017). The coefficients 0.1 and 1.25 were used to adjust for sparsely vegetated or barren land and have been evaluated using the SIF data.

The maximum light used efficiency values for C₃ croplands ($\epsilon_{\max\text{-C}_3}$) and C₄ croplands ($\epsilon_{\max\text{-C}_4}$) were specified as 0.035 mol CO₂ mol⁻¹ PAR (~1.8 g·C·m⁻²·day⁻¹·MJ⁻¹·(PAR)), and 0.053 mol CO₂ mol⁻¹ (PAR) (~2.7 g·C·m⁻²·day⁻¹·MJ⁻¹·(PAR)) (1.5 times larger than C₃ types), respectively (Li et al., 2013). T_{scalar} and W_{scalar} are the temperature and water regulation factor and calculated as

$$T_{\text{scalar}} = \frac{(T - T_{\min})(T - T_{\max})}{[(T - T_{\min})(T - T_{\max})] - (T - T_{\text{opt}})^2}, \quad (3)$$

$$W_{\text{scalar}} = \frac{1 + \text{LSWI}}{1 + \text{LSWI}_{\max}}, \quad (4)$$

where T is the air temperature, derived from the NCEP/North American Regional Reanalysis (NARR) climate data. T_{\min} , T_{\max} , and T_{opt} represent the minimum, maximum, and optimum temperatures for photosynthesis, respectively, which are biome-specific and assigned values as in Zhang, Xiao, Jin, et al. (2016). LSWI_{\max} is the maximum land surface water index (LSWI) within the plant growing season, and we applied a temporal smoothing method using nearby 4 years (2 years before and 2 years after) to eliminate potential bias (Zhang et al., 2017).

2.2. Input Data Sets for VPM Simulations in CONUS During 2008–2014

Regional simulations of VPM model require climate, vegetation indices, and land cover data. Here we briefly describe the input data sets used: (1) NCEP/NARR reanalysis meteorological data, (2) Moderate Resolution Imaging Spectroradiometer (MODIS) surface reflectance and land cover data, and (3) NASS CDL data.

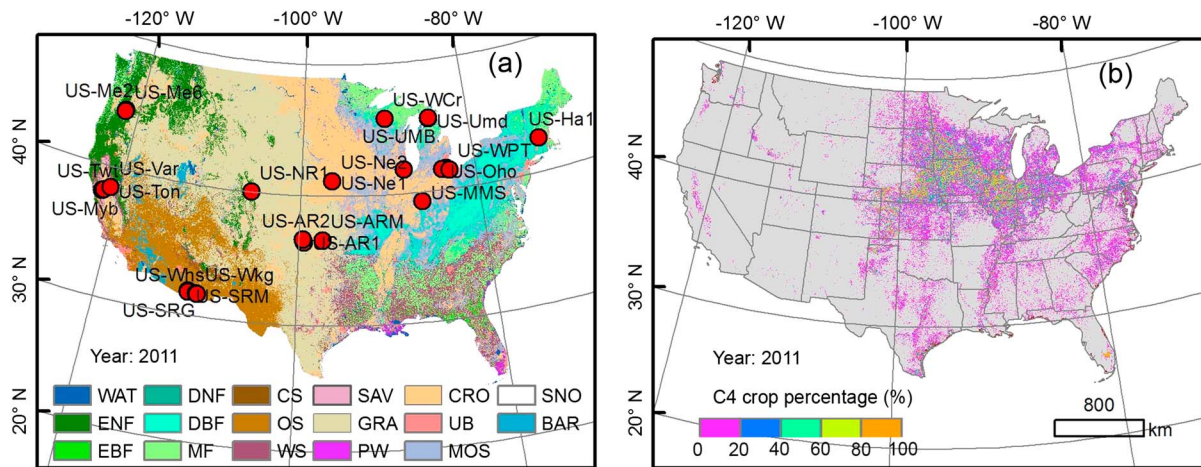


Figure 1. (a) Land cover map of Contiguous United States derived from MCD12Q1 in 2011 and (b) the C_4 crop percentage within a 500-m Moderate Resolution Imaging Spectroradiometer pixel derived from 30-m cropland data layer. Abbreviations denote the International Geosphere-Biosphere Programme land use classes. WAT = Water; ENF = Evergreen Needleleaf Forest; EBF = Evergreen Broadleaf Forest; DNF = Deciduous Needleleaf Forest; DBF = Deciduous Broadleaf Forest; MF = Mixed Forest; CS = Closed Shrublands; OS = Open Shrublands; WS = Woody Shrublands; SAV = Savannas; GRA = Grasslands; PW = permanent wetlands; CRO = Croplands; UB = Urban and Built-up; MOS = Cropland/Natural vegetation mosaic; SNO = Snow and Ice; BAR = Barren or sparsely vegetated. In (a), we also labeled the locations of the eddy covariance flux tower sites used in this study.

2.2.1. NCEP/NARR Climate Data

The NCEP/NARR data were downloaded from (<http://www.esrl.noaa.gov/psd>). It contains meteorological variables such as air temperature, precipitation, and downward shortwave radiation from 1979 to present at a spatial resolution of 32 km and a temporal resolution of 3 hr. The original 3-hourly NARR data were aggregated into daily data by calculating the maximum, mean, and minimum air temperature in a day ($^{\circ}\text{C}$) and the cumulative sum of downward shortwave radiation in a day. The resulting daily data were further aggregated to 8-day intervals (following the MODIS 8-day temporal resolution) by calculating the maximum, mean, and minimum temperature ($^{\circ}\text{C}$) and the cumulative sum of downward shortwave radiation within an 8-day period. We also interpolated these climate variables (32-km spatial resolution) to 500 m using the same algorithm reported in a previous publication (Zhang, Xiao, Jin, et al., 2016). As previous studies have shown, the NARR downward shortwave radiation is systematically overestimated, so we adjusted it by applying a correction factor of 0.8 as proposed in a previous study (Jin et al., 2015).

2.2.2. MODIS Surface Reflectance and Land Cover Product

The latest version of MODIS surface reflectance product, MOD09A1 V006, was used to calculate EVI (Huete et al., 1997) and LSWI (Xiao, Zhang, et al., 2004). A temporal algorithm was applied to EVI to gap-fill the missing data or bad-quality data (Zhang, Xiao, Jin, et al., 2016).

The MODIS land cover product (MCD12Q1 V005) provides annual global maps of land cover at 500-m spatial resolution during 2001–2013 (Friedl et al., 2010). We used the MCD12Q1 data at 2013 to represent year 2014. The International Geosphere-Biosphere Programme land cover classification scheme in the MCD12Q1 is used in this study (see Figure 1a). The International Geosphere-Biosphere Programme land cover map was then used to derive biome-specific model parameter information for VPM simulations.

2.2.3. USDA NASS CDL Data Set

Annual national CDL data sets with a spatial resolution of 30 m were available for our study period (2008–2014; https://www.nass.usda.gov/Research_and_Science/Cropland/SARS1a.php). The CDL data sets contain over 100 cropland types and have very high classification accuracies for most crops (over 90% accuracy for major crop types such as soybean and corn; Boryan et al., 2011). For the VPM simulations, annual CDL data sets in 2008–2014 were aggregated to generate data layers at 500-m spatial resolution that represent the ratio of C_3 and C_4 vegetation within individual 500-m gridcells for each year (Figure 1b). The C_4 cropland layer included corn, sorghum, sugarcane, and millet, and all other crops were C_3 .

2.3. Evaluation of GPP Estimates During 2008–2014 From VPM

2.3.1. GPP Data From EC Flux Tower Sites

EC data from the FLUXNET2015 data set were used to assess GPP_{VPM} . We used 25 FLUXNET sites across CONUS according to their data availability during 2008–2014, for which a summary about these sites is shown in Table 1 and Figure 1a. The FLUXNET2015 data set used a standard workflow to process the data from the EC flux tower sites (<http://fluxnet.fluxdata.org/data/>). The net ecosystem exchange of CO_2 between ecosystems and the atmosphere was gap-filled and then partitioned into GPP and ER using two methods, the nighttime-based and the daytime-based approaches (Lasslop et al., 2010; Reichstein et al., 2005). We calculated average daily GPP_{EC} as the average of daily GPP estimated by the two methods. Then, we calculated 8-day average GPP_{EC} by aggregating the average daily GPPs. For each 8-day interval, only the shortwave radiation and net ecosystem exchange observations with more than 75% of good quality, gap-filled data were kept.

We evaluated the seasonal and cross-site performance of GPP_{VPM} across biomes at 8-day and interannual scales. We classified the land cover maps into four major types: forest (FOR), grassland (GRA), cropland (CRO), and others (OTH) based on the MCD12Q1 landcover data. The evergreen needleleaf forest, evergreen broadleaf forest, deciduous broadleaf forest, deciduous needleleaf forest, and mixed forest were lumped together as forest. Grassland and cropland were the same classification scheme as MCD12Q1, while all the other land cover types, such as savannas, shrublands, wetlands, and sparsely vegetated area, were considered as OTH. To examine the ability of the model to capture the interannual variability of GPP, we compared the anomaly of annual GPP for GPP_{EC} and GPP_{VPM} . Specifically, we compared GPP_{VPM} and GPP_{MOD17} to the anomaly between GPP_{EC} in each site year and average GPP_{EC} over all the site years for each site. The slope, root mean square error (RMSE), and R^2 of the regression models were used to evaluate the difference between modeled and eddy covariance-derived GPP.

2.3.2. SIF Data From the GOME-2

SIF is a very small amount of energy emitted by plants and has been demonstrated to be highly correlated with GPP (Guanter et al., 2014; Wagle et al., 2016; Zhang, Xiao, Jin, et al., 2016). In this study, we used the monthly GOME-2 SIF data (V26) during 2008–2014 (Joiner et al., 2013). GOME-2 measurements are in the ultraviolet and visible part of the spectrum (240–790 nm) with a high spectral resolution between 0.2 and 0.5 nm and with the footprint size of $80 \times 40 \text{ km}^2$. SIF is retrieved using a principle component analysis method in the 734 to 758 nm spectral window which overlaps the second peak of the SIF emission. The retrievals are quality-filtered and aggregated into 0.5° grids and a monthly interval (Joiner et al., 2013).

2.4. Inter-Comparison of GPP Estimates Among VPM and Other Three Models

We compared GPP_{VPM} with the latest version of MOD17 GPP product (Running et al., 2004), MOD17A2H V006 (GPP_{MOD17}) at both site and regional scales. GPP_{MOD17} is estimated at a spatial resolution of 500 m and a temporal resolution of 8 days, which matches the spatial and temporal resolutions of GPP_{VPM} . MOD17 is also a LUE model and simulates GPP as the product of $APAR_{canopy}$ and light use efficiency (ϵ_g). ϵ_g is determined by ϵ_{max} and scalars that capture environmental limitations such as vapor pressure deficit (VPD) and air temperature. ϵ_{max} values are specific for different biome types (e.g., forest, shrub, grass, crop; Running et al., 2004), but the product does not account for the differences of ϵ_{max} between C_3 and C_4 croplands, and ϵ_{max} for croplands is substantially too low (Turner et al., 2006; Xin et al., 2015).

We also compared GPP_{VPM} with GPP simulated by CASA-GFED3 (GPP_{CASA}). CASA estimates Net Primary Productivity (NPP) based on the light use efficiency method (Monteith, 1972, 1977) and further estimates GPP with an assumption $GPP = 2 * NPP$. ϵ_{max} for predicting NPP in CASA is set uniformly ($0.55 \text{ g-C-MJ}^{-1}\text{-PAR}$) for different biomes (Potter et al., 1993, 2012; Randerson et al., 1996). The CASA-GFED3 GPP product used a calibrated ϵ_{max} for the Midwestern region, which was derived from crop yield observations, meteorological data, and remotely sensed FPAR (Lobell et al., 2002), and thus corresponds with much higher GPP values (roughly 45%) over the Midwestern United States (Hilton et al., 2015). GPP_{CASA} is used to generate prior biogenic CO_2 fluxes for the CarbonTracker system (Peters et al., 2007) at a spatial resolution of $1^\circ \times 1.25^\circ$ every 3 hr. We resampled the data into $1^\circ \times 1^\circ$ and aggregated them into monthly values in this study.

Table 1
Name, Location, Vegetation Type, and Available Years (Within 2008–2014 Study Period) of 25 Eddy Covariance Flux Tower Sites in This Study

Site ID	Latitude	Longitude	IGBP	Time	Slope		R^2		RMSE ($\text{g}\cdot\text{C}\cdot\text{m}^{-2}\cdot\text{day}^{-1}$)		References	DOI
					VPM	MOD17	VPM	MOD17	VPM	MOD17		
US-Ha1	42.5378	-72.1715	DBF	2009–2012	0.93	0.66	0.93	0.74	1.32	2.89	Urbanski et al. (2007)	https://doi.org/10.17190/AMF/1246059
US-MMS	39.3232	-86.4131	DBF	2009–2014	1.07	0.85	0.91	0.71	1.58	2.33	Schmid et al. (2000)	https://doi.org/10.17190/AMF/1246080
US-Oho	41.5545	-83.8438	DBF	2009–2013	0.87	0.77	0.92	0.83	1.63	2.37	van Gorsel et al. (2009)	https://doi.org/10.17190/AMF/1246089
US-UMB	45.5598	-84.7138	DBF	2009–2014	1.09	1.20	0.96	0.93	1.15	1.87	Gough et al. (2008)	https://doi.org/10.17190/AMF/1246107
US-Umd	45.5625	-84.6975	DBF	2009–2014	0.91	0.90	0.88	0.84	1.64	1.70	Gough et al. (2013)	https://doi.org/10.17190/AMF/1246134
US-WCr	45.8059	-90.0799	DBF	2011–2014	1.25	0.84	0.90	0.80	2.46	2.03	Cook et al. (2004)	https://doi.org/10.17190/AMF/1246111
US-Me2	44.4523	-121.5574	ENF	2009–2014	0.58	0.72	0.74	0.79	2.81	2.08	Law et al. (2004)	https://doi.org/10.17190/AMF/1246076
US-Me6	44.3233	-121.6078	ENF	2010–2014	0.56	0.95	0.51	0.56	1.53	1.26	Law et al. (2000)	https://doi.org/10.17190/AMF/1246128
US-NR1	40.0329	-105.5464	ENF	2009–2014	0.84	0.91	0.86	0.84	1.04	1.03	Monson et al. (2002)	https://doi.org/10.17190/AMF/1246088
US-SRM	31.8214	-110.8661	WSA	2009–2014	0.90	0.61	0.74	-1.18	0.49	0.81	Scott et al. (2009)	https://doi.org/10.17190/AMF/1246104
US-Ton	38.4316	-120.9660	WSA	2009–2014	0.68	1.01	0.61	0.73	1.28	0.91	Baldocchi et al. (2004)	https://doi.org/10.17190/AMF/1246137
US-AR1	36.4267	-99.4200	GRA	2009–2012	1.07	0.59	0.55	0.06	1.35	1.35	-	https://doi.org/10.17190/AMF/1246131
US-AR2	36.6358	-99.5975	GRA	2009–2012	1.08	0.62	0.43	-0.12	1.14	1.20	-	https://doi.org/10.17190/AMF/1246138
US-IB2	41.8406	-88.2410	GRA	2009–2011	1.21	0.84	0.87	0.86	2.14	1.52	Matamala et al. (2008)	https://doi.org/10.17190/AMF/1246066
US-SRG	31.7894	-110.8277	GRA	2009–2014	0.78	0.51	0.69	-0.35	0.75	1.16	Scott et al. (2015)	https://doi.org/10.17190/AMF/1246154
US-Var	38.4133	-120.9507	GRA	2009–2014	0.66	0.88	0.66	0.42	1.71	1.65	Ma et al. (2007)	https://doi.org/10.17190/AMF/1245984
US-Wkg	31.7365	-109.9419	GRA	2009–2014	0.76	0.63	0.82	0.39	0.54	0.69	Scott et al. (2010)	https://doi.org/10.17190/AMF/1246112
US-ARM	36.6058	-97.4888	CRO	2009–2012	0.79	0.64	0.57	0.47	1.46	1.56	Fischer et al. (2007)	https://doi.org/10.17190/AMF/1246027
US-CRT	41.6285	-83.3471	CRO	2011–2013	0.68	0.45	0.78	0.64	3.00	4.23	Chu et al. (2014)	https://doi.org/10.17190/AMF/1246156
US-Ne1	41.1651	-96.4766	CRO	2009–2012	0.96	0.31	0.95	0.51	1.80	7.62	Suyker et al. (2005)	https://doi.org/10.17190/AMF/1246084
US-Ne2	41.1649	-96.4701	CRO	2009–2012	0.89	0.29	0.96	0.41	1.90	8.19	Suyker et al. (2005)	https://doi.org/10.17190/AMF/1246085
US-Twt	38.1087	-121.6530	CRO	2009–2014	0.87	0.53	0.43	-0.93	3.17	4.24	Hatala et al. (2012)	https://doi.org/10.17190/AMF/1246140
US-SRC	31.9083	-110.8395	OSH	2009–2014	0.97	0.99	0.32	-1.31	0.39	0.42	Cavanaugh et al. (2011)	https://doi.org/10.17190/AMF/1246127
US-Whs	31.7438	-110.0522	OSH	2009–2014	0.70	0.71	0.72	-0.28	0.45	0.56	Scott et al. (2015)	https://doi.org/10.17190/AMF/1246113
US-Myb	38.0498	-121.7651	WET	2011–2014	1.27	0.92	0.36	-0.31	3.49	2.85	Sturtevant et al. (2016)	https://doi.org/10.17190/AMF/1246139

Note. RMSE, R^2 , and slope are the root mean square error, coefficient of determination, and regression slope of the regression analysis, respectively, between tower-derived gross primary production and simulated gross primary production from VPM and MOD17. IGBP = International Geosphere-Biosphere Programme; VPM = Vegetation Photosynthesis Model; DBF = Deciduous Needleleaf Forest; ENF = Evergreen Needleleaf Forest; GRA = grassland; CRO = cropland.

The GPP estimates by the SiBCASA-GFED4 model ($GPP_{SiBCASA}$; van der Velde et al., 2014) were also compared with regional GPP_{VPM} . $GPP_{SiBCASA}$ is used to generate prior biogenic CO_2 fluxes in the Carbon Tracker Europe system (van der Laan-Luijkx et al., 2017). SiBCASA combines the biophysical and GPP components from the Simple Biosphere model (version 2.5) with the heterotrophic respiration (R_H) from CASA model and calculates the exchange of carbon, energy, and water at a temporal resolution of 10 min and at a spatial resolution of $1^\circ \times 1^\circ$ (Schaefer et al., 2008; van der Velde et al., 2014). GPP is calculated for both C_3 and C_4 plants by implementing a modified version of the C_3 enzyme kinetic model (Farquhar et al., 1980) and the C_4 photosynthesis model (Collatz et al., 1992). The C_4 distribution map used in SiBCASA is a static map with the mean C_4 fraction in global $1^\circ \times 1^\circ$ grids (Still et al., 2003). The aggregated monthly $GPP_{SiBCASA}$ data are used for the comparison.

The impact of climate extremes on the GPP and SIF over the CONUS was evaluated using the four GPP data sets and GOME-2 SIF data. The seasonal cycle and anomaly of GPP_{VPM} , GPP_{MOD17} , $GPP_{SiBCASA}$, GPP_{CASA} , and SIF in the year 2012 were compared to that in the baseline year (the average of the year 2008, 2009, 2010, 2013, and 2014). The uncertainty range of the anomaly was calculated as the standard deviation of the anomaly between 2012 and selected different baselines. We randomly chose at least 3 years from the year 2008, 2009, 2010, 2013, and 2014 to calculate the baseline, so there are 16 options ($C_3^3 + C_3^4 + C_3^5$). As $GPP_{SiBCASA}$, GPP_{CASA} , and SIF data sets have a spatial resolution of $1.0^\circ \times 1.0^\circ$, both GPP_{VPM} and GPP_{MOD17} data sets (500-m spatial resolution) were aggregated to $1.0^\circ \times 1.0^\circ$. The SIF data ($0.5^\circ \times 0.5^\circ$) were also aggregated to $1.0^\circ \times 1.0^\circ$. We then used the area-weighted method to calculate annual total GPP (pg C per year) and average SIF over CONUS.

3. Results

3.1. Seasonal Dynamics and Interannual Variation of GPP at Flux Tower Sites

GPP_{VPM} agreed reasonably well with the seasonal dynamics and peak values of GPP_{EC} at most sites (Figure 2). The coefficients of determination (R^2) varied from 0.32 (US-SRC site) to 0.96 (US-Ne2 and US-UMB). GPP_{VPM} showed very high accuracy for the cropland sites relative to GPP_{MOD17} (see Figure 2 and Table 1). At the US-Ne1 and US-Ne2 maize sites, the regression between GPP_{VPM} and GPP_{EC} show a high R^2 value (>0.95) and a low RMSE value ($<2.0 \text{ g-C}\cdot\text{m}^{-2}\cdot\text{day}^{-1}$), while the regression between GPP_{MOD17} and GPP_{EC} shows a moderate R^2 value (~ 0.50) and a large RMSE value ($7.0 \text{ g-C}\cdot\text{m}^{-2}\cdot\text{day}^{-1}$; Table 1).

At the 8-day scale, GPP_{VPM} agrees better with GPP_{EC} than does GPP_{MOD17} , and GPP_{VPM} effectively captures the seasonal dynamics of GPP for all the four biomes (Figures 3a and 3b). For croplands, GPP_{MOD17} shows significant underestimation with a slope of 0.37, while GPP_{VPM} presents only slight underestimation with a slope of 0.97. The improvement in GPP_{VPM} is most prominent in these C_4 cropland sites, such as US-Ne1 and US-Ne2 (Figure 2 and Table 1), with peak value of GPP_{VPM} and GPP_{EC} in the growing season that are larger than $20 \text{ g-C}\cdot\text{m}^{-2}\cdot\text{day}^{-1}$, while that of GPP_{MOD17} is less than $10 \text{ g-C}\cdot\text{m}^{-2}\cdot\text{day}^{-1}$. Across all 25 sites, GPP_{VPM} explains about 84% of the seasonal dynamics of GPP_{EC} with RMSE of $1.7 \text{ g-C}\cdot\text{m}^{-2}\cdot\text{day}^{-1}$, while GPP_{MOD17} only explains only about 55% with a RMSE value of $2.6 \text{ g-C}\cdot\text{m}^{-2}\cdot\text{day}^{-1}$.

The interannual variation of GPP_{VPM} was best for croplands, followed by forest, grasslands, and other biomes (Figure 3c). In addition, the anomaly of annual GPP_{VPM} in croplands, grasslands, and forest biomes has much higher consistency with GPP_{EC} than does GPP_{MOD17} (Figures 3c and 3d). In other biomes (five sites), both GPP_{VPM} and GPP_{MOD17} had relatively low accuracy.

3.2. Spatial–Temporal Consistency Between Model-Based GPP and SIF Over CONUS in the Baseline Years and Drought Year 2012

We compared the spatial distribution of maximum monthly mean GPP ($\text{g-C}\cdot\text{m}^{-2}\cdot\text{day}^{-1}$) from the four GPP products and annual maximum monthly mean SIF in the baseline year and drought year 2012 at $1^\circ \times 1^\circ$ resolution (Figures 4a–4j). The maximum monthly mean GPP in 2008, 2009, 2010, 2013, and 2014 were used as baseline year. The three GPP products (GPP_{VPM} , GPP_{CASA} , and $GPP_{SiBCASA}$) and SIF show the peak photosynthesis in the Midwestern corn-belt region (Figures 4a–4j), which was consistent with the results reported by Hilton et al. (2017). GPP_{MOD17} did not have such a spatial pattern for maximum monthly GPP because it did not include higher photosynthetic capacity for C_4 vegetation as did the other three models (VPM, CASA, and SiBCASA). Compared to the baseline years, most of gridcells had lower GPP and SIF values

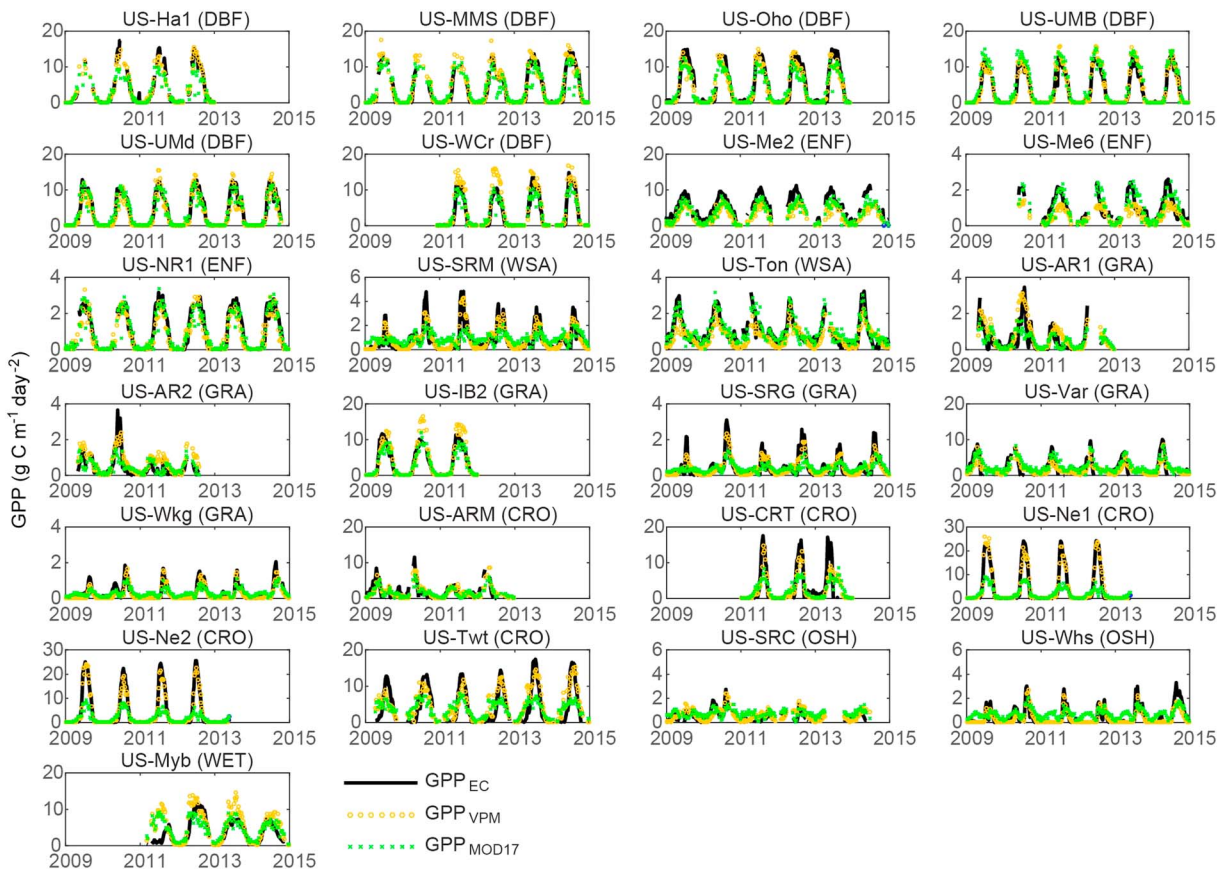


Figure 2. Seasonal dynamics and interannual variations of the tower-based GPP (GPP_{EC}), GPP simulated by VPM (GPP_{VPM}), and GPP simulated by MOD17 (GPP_{MOD17}) at 25 flux sites at 8-day intervals (please note the different y axis scales). DBF = Deciduous Needleleaf Forest; ENF = Evergreen Needleleaf Forest; GRA = grassland; CRO = cropland; EC = eddy covariance; VPM = Vegetation Photosynthesis Model; GPP = gross primary production.

during the drought in 2012. The correlation analysis (Figures 5a–5d and 5e–5h) showed that the maximum monthly GPP_{VPM} and SIF have the strongest linear relationship, followed by $SIF/GPP_{SiBCASA}$, SIF/GPP_{CASA} , and SIF/GPP_{MOD17} .

For annual total GPP, all four GPP products showed very similar spatial patterns with SIF, with relatively high annual GPP ($>1,500 \text{ g-C-m}^{-2}\cdot\text{year}^{-1}$) in the forested Southeastern United States and low annual GPP in the western regions where grasslands and deserts are dominant (Figures 4k–4t). In 2012, GPP_{VPM} had a decrease in the Midwestern corn-belt region and Great Plains and an increase in the eastern temperate forest region, which is consistent with the spatial patterns of SIF. Annual GPP_{MOD17} had an obvious decrease in the Midwestern corn-belt area but a slight increase in the eastern forest area in 2012. Annual $GPP_{SiBCASA}$ had no significant differences between the baseline and drought year 2012. Annual GPP_{CASA} had large increases in both the Midwestern corn-belt region and temperate forest area. The correlation analysis (Figures 5i–5l) showed that annual GPP_{VPM} had a stronger linear relationship with SIF ($R^2 = 0.94$) in the baseline years than $SIF/GPP_{SiBCASA}$ ($R^2 = 0.76$), SIF/GPP_{CASA} ($R^2 = 0.75$), and SIF/GPP_{MOD17} ($R^2 = 0.70$). We found similar results for the drought year 2012 (Figures 5m–5p), which suggested that the models performed similarly during baseline and drought years.

GPP estimates from all models had a high correlation with SIF (>0.9) in the wetter eastern region but a low correlation in the dry western region, partly due to the very low SIF signal and relatively large signal-to-noise ratio (Figures 6a–6h). The percentages of the total number of gridcells with a Pearson correlation coefficient larger than 0.9 in the baseline year were $\sim 65\%$ for SIF/GPP_{VPM} , $\sim 55\%$ for SIF/GPP_{CASA} , $\sim 50\%$ for SIF/GPP_{MOD17} , and $\sim 47\%$ for $SIF/GPP_{SiBCASA}$ (Figures 6i–6l). The four GPP models had no obvious differences in simulating the seasonal dynamics of GPP between the baseline year and drought year 2012 (Figure 6).

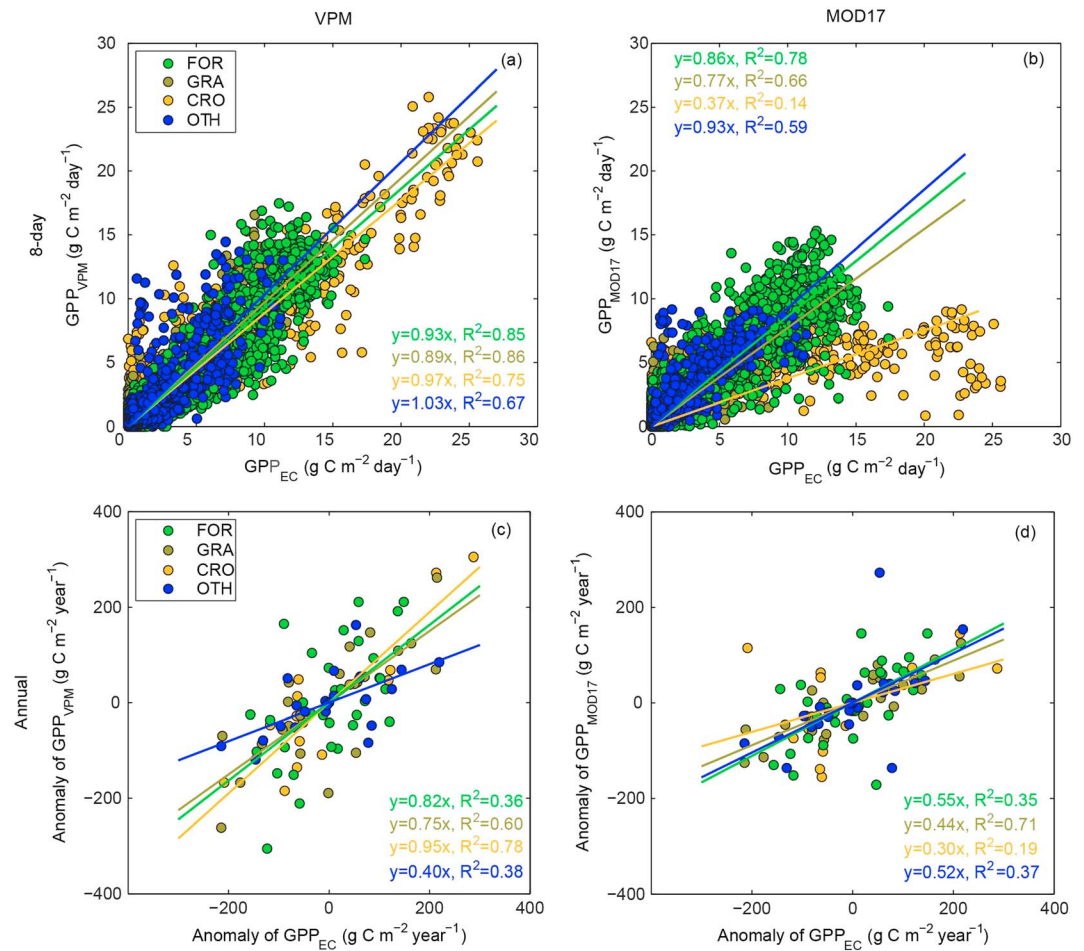


Figure 3. Comparison of GPP_{EC}, GPP_{VPM}, and GPP_{MOD17} across eddy covariance flux tower sites (FO, GRA, CRO, and OTH) during 2008 to 2014: (a) 8-day GPP_{EC} and GPP_{VPM}, (b) 8-day GPP_{EC} and GPP_{MOD17}, (c) anomaly of annual GPP_{EC} and GPP_{VPM}, and (d) anomaly of annual GPP_{EC} and GPP_{MOD17}. FOR = forests; CRO = croplands; GRA = grasslands; OTH = other types. When all the sites were combined, the relationship between GPP_{VPM} and GPP_{EC} was $y = 0.92x$ ($R^2 = 0.84$, $RMSE = 1.7 \text{ g}\cdot\text{C}\cdot\text{m}^{-2}\cdot\text{day}^{-1}$) at the 8-day time scale, while the relationship between GPP_{MOD17} and GPP_{EC} was $y = 0.68x$ ($R^2 = 0.55$, $RMSE = 2.6 \text{ g}\cdot\text{C}\cdot\text{m}^{-2}\cdot\text{day}^{-1}$) at the 8-day time scale. At the interannual scale, the relationship between the annual anomaly of GPP_{VPM} and GPP_{EC} is $y = 0.73x$ ($R^2 = 0.48$), while the relationship between the annual anomaly of GPP_{MOD17} and GPP_{EC} was $y = 0.45x$ ($R^2 = 0.37$). GPP = gross primary production; VPM = Vegetation Photosynthesis Model; EC = eddy covariance; RMSE = root mean square error.

The histograms of the slope values ($GPP = a \times SIF + b$) among these four GPP models differed substantially. The slope values for the SIF/GPP_{VPM} were concentrated between 4 and 7 $\text{g}\cdot\text{C}\cdot\text{mW}^{-1}\cdot\text{nm}^{-1}\cdot\text{sr}^{-1}$ (~53% of all gridcells), while that for SIF/GPP_{MOD17} were between 2 and 5 $\text{g}\cdot\text{C}\cdot\text{mW}^{-1}\cdot\text{nm}^{-1}\cdot\text{sr}^{-1}$ (~60% of all gridcells). The slope values for the SIF/GPP_{CASA} and SIF/GPP_{SIBCASA} were more evenly distributed than that of SIF/GPP_{VPM}. Sun et al. (2017) found the GPP-SIF relationship is consistent across different vegetation types when comparing SIF with GPP_{EC}, but it is more divergent when comparing SIF with modeled GPP because of the systematic GPP biases. The GPP-SIF slope for the four GPP products in this study is also divergent over CONUS, but the VPM GPP-SIF slope is more convergent than the other three models (Figure 7).

3.3. Spatial-Temporal Consistency of GPP and SIF Anomalies Over CONUS in 2012

To evaluate the impacts of spring warming and summer drought on GPP in 2012, we compared the anomalies of GPP from GPP_{VPM}, GPP_{MOD17}, GPP_{SIBCASA}, and GPP_{CASA} to the anomalies of SIF in the spring, summer, and the entire year at $1^\circ \times 1^\circ$ (latitude and longitude) resolution (Figure 8). The anomalies of GPP and SIF were calculated as the differences between year 2012 and the baseline year. The baseline year was calculated as

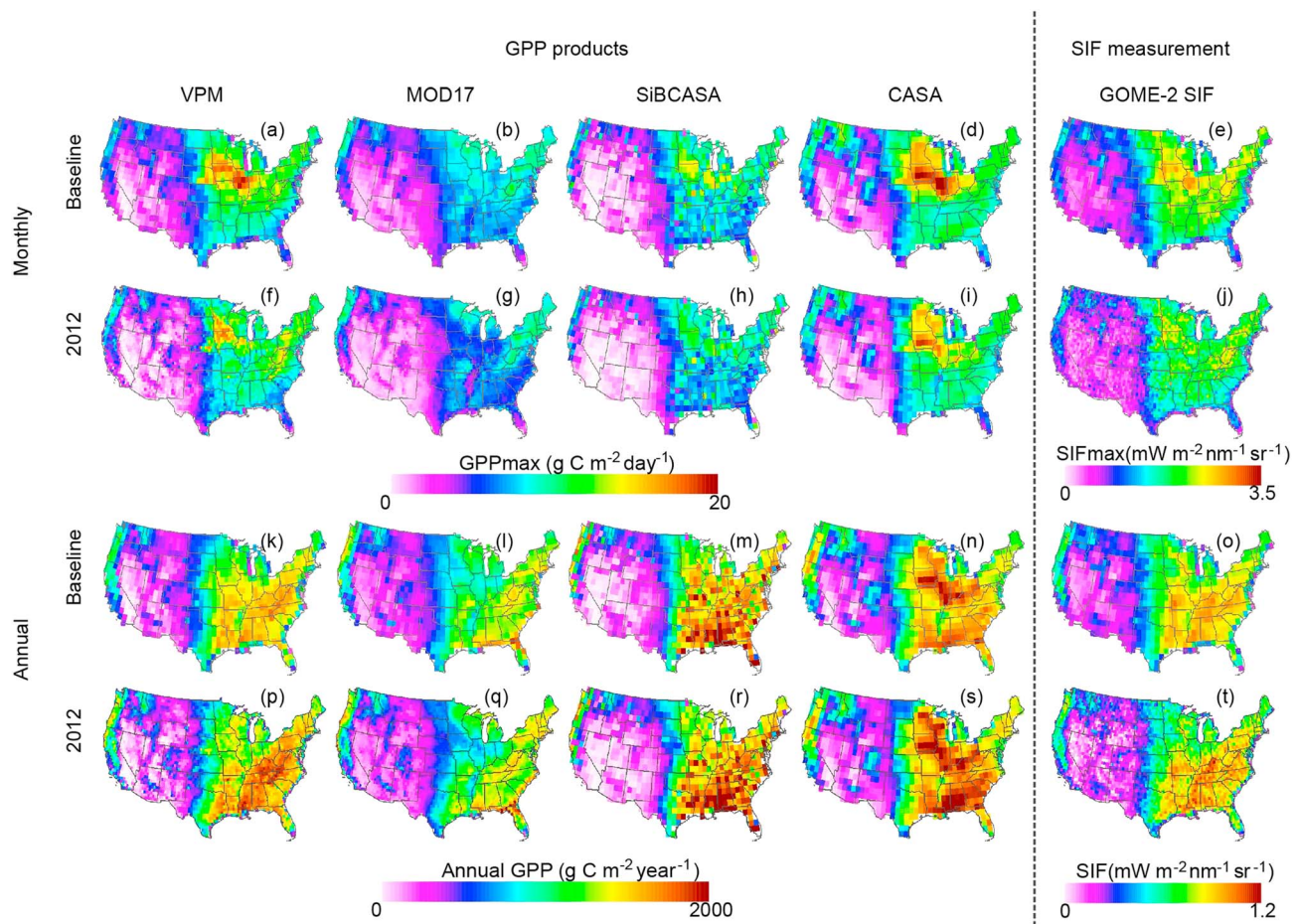


Figure 4. Spatial distribution of maximum monthly mean GPP (a–d; f–i) from GPP models (VPM, MOD17, SiB-CASA, and CASA) and maximum monthly mean SIF (e, j) from GOME-2 (e, j) in the baseline years (the average of 2008, 2009, 2010, 2013, and 2014) and drought year 2012, and spatial distributions of annual GPP (k–n; p–s) from GPP models and annual mean SIF from GOME-2 (o, t) in the baseline years and drought year 2012. VPM = Vegetation Photosynthesis Model; CASA = Carnegie-Ames-Stanford Approach; SiBCASA = Simple Biosphere/CASA; GOME-2 = Global Ozone Monitoring Experiment-2; SIF = solar-induced chlorophyll fluorescence; GPP = gross primary production.

the average of 2008, 2009, 2010, 2013, and 2014. Geographically, the anomaly of all the four GPP products and SIF showed very interesting spatial patterns at the seasonal and annual scales (Figure 8).

In the spring season, the middle and eastern CONUS experienced an increase in GPP anomaly while western CONUS experienced a decrease, which was consistent with the spatial pattern of SIF anomaly (Figures 8a–8e). The magnitudes and spatial extent of GPP anomaly vary among the four GPP models. For GPP_{VPM} and GPP_{MOD17} , the large increases in GPP (larger than $100 \text{ g-C-m}^{-2}\cdot\text{season}^{-1}$) occurred mostly in the Southern Great Plains and part of the Midwestern corn-belt region. For GPP_{CASA} , large increases in GPP occurred mostly in the Midwestern and Southeast regions. The correlation analyses between GPP products and SIF (Figures 9a–9d) showed that GPP_{VPM} and SIF had the strongest linear relationship ($R^2 = 0.67$), followed by SIF/GPP_{MOD17} ($R^2 = 0.58$), SIF/GPP_{CASA} ($R^2 = 0.56$), and $SIF/GPP_{SiBCASA}$ ($R^2 = 0.48$).

In the summer season, most regions in CONUS experienced decreased GPP and SIF associated with drought (Figures 8f–8j). The Great Plains and Midwestern corn-belt regions experienced the largest reductions in GPP (larger than $150 \text{ g-C-m}^{-2}\cdot\text{season}^{-1}$). The spatial extents of decreased GPP in GPP_{VPM} and GPP_{MOD17} were greater than those in $GPP_{SiBCASA}$ and GPP_{CASA} . GPP_{VPM} , GPP_{CASA} , and $GPP_{SiBCASA}$ displayed strong increases in the southeast regions, which was consistent with the spatial pattern of SIF anomaly. Overall, GPP_{VPM} (Figures 9e–9h) agreed best with SIF ($R^2 = 0.71$), followed by SIF/GPP_{CASA} ($R^2 = 0.50$), SIF/GPP_{MOD17} ($R^2 = 0.45$), and $SIF/GPP_{SiBCASA}$ ($R^2 = 0.19$).

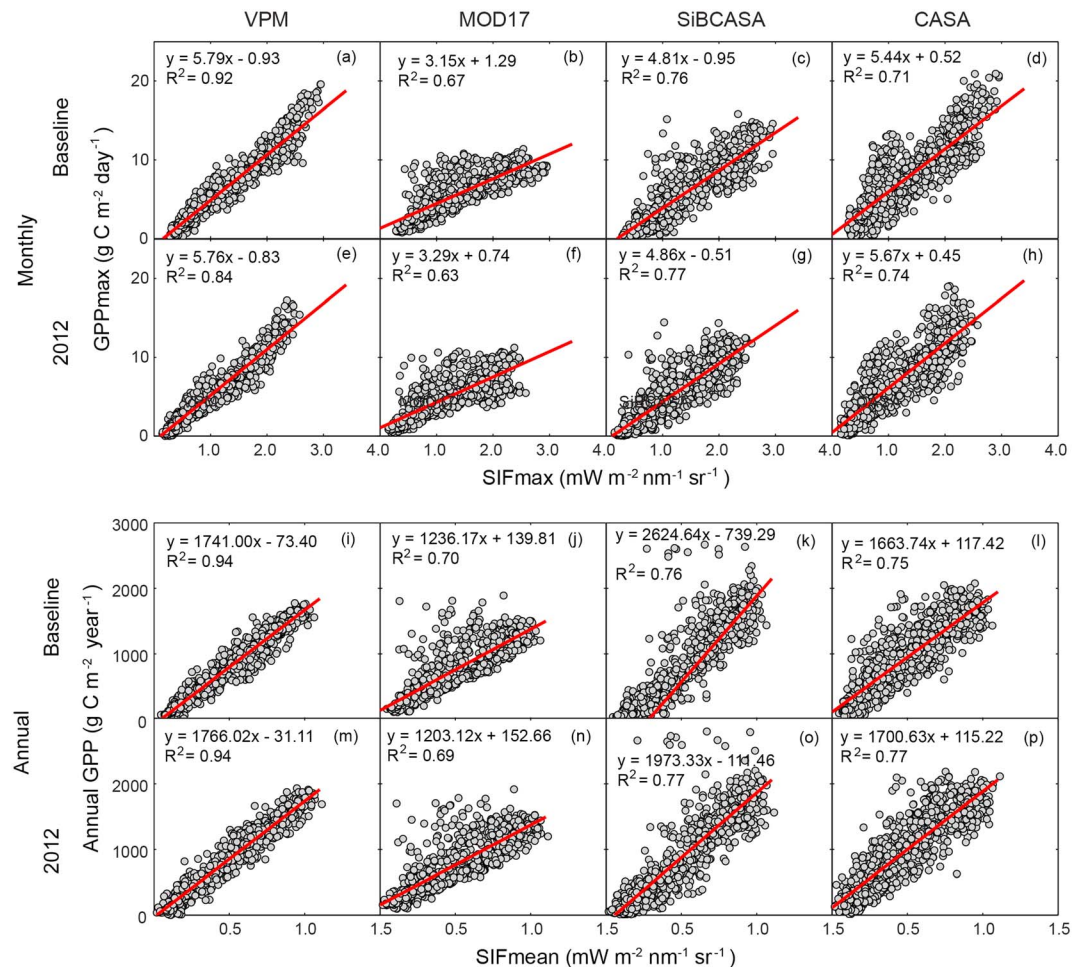


Figure 5. Relationships between the maximum monthly mean GPP (a–d; e–h) from GPP models (VPM, MOD17, SiBCASA, and CASA) and monthly mean SIF from Global Ozone Monitoring Experiment-2 for each pixel across Contiguous United States during the baseline years (the average of 2008, 2009, 2010, 2013, and 2014) and drought year 2012, and relationship between total annual GPP (i–l; m–p) from GPP models (VPM, MOD17, SiBCASA, and CASA) and mean annual SIF from Global Ozone Monitoring Experiment-2 in the baseline year (the average of 2008, 2009, 2010, 2013, and 2014) and drought year 2012 (all of the relationships are significant with $p < 0.001$). GPP = gross primary production; VPM = Vegetation Photosynthesis Model; CASA = Carnegie-Ames-Stanford Approach; SiBCASA = Simple Biosphere/CASA; SIF = solar-induced chlorophyll fluorescence.

For the entire year, annual GPP_{VPM}, GPP_{MOD17}, and GPP_{SiBCASA} mainly decreased in the western United States and corn-belt regions, and annual GPP increased mainly in the eastern and southern forest area, which was consistent with the spatial pattern of SIF (Figures 8k–8o). Only GPP_{CASA} reported strong increases in GPP in the corn-belt region. The correlation analysis showed that none of the four GPP products agreed well with the spatial pattern of annual mean SIF anomaly at the annual scale, with R^2 values varying from 0.14 to 0.27 (Figures 9i–9l).

When aggregated over the entire CONUS by season, the four GPP products and SIF clearly showed an increase in GPP in the spring and a reduction in the summer, indicating the warm spring and droughty summer had opposite effects on GPP (Figure 8 and Table 2). The spring warming led to an increase in GPP by 0.25–0.48 pg C per season, where GPP_{CASA} showed the largest increase and GPP_{SiBCASA} showed the least. During the summer, the four GPP products showed a decrease in GPP by 0.21–0.42 pg C per season, where GPP_{CASA} decreased the most and GPP_{SiBCASA} decreased the least. The annual total GPP_{VPM} and GPP_{CASA} had an increase of 0.11 and 0.18 pg C per year, while the annual total GPP_{MOD17} and mean SIF had a decrease of 0.12 pg C per year and 0.12 mW·m⁻²·nm⁻¹·sr⁻¹. The annual total GPP_{SiBCASA} remained neutral in 2012.

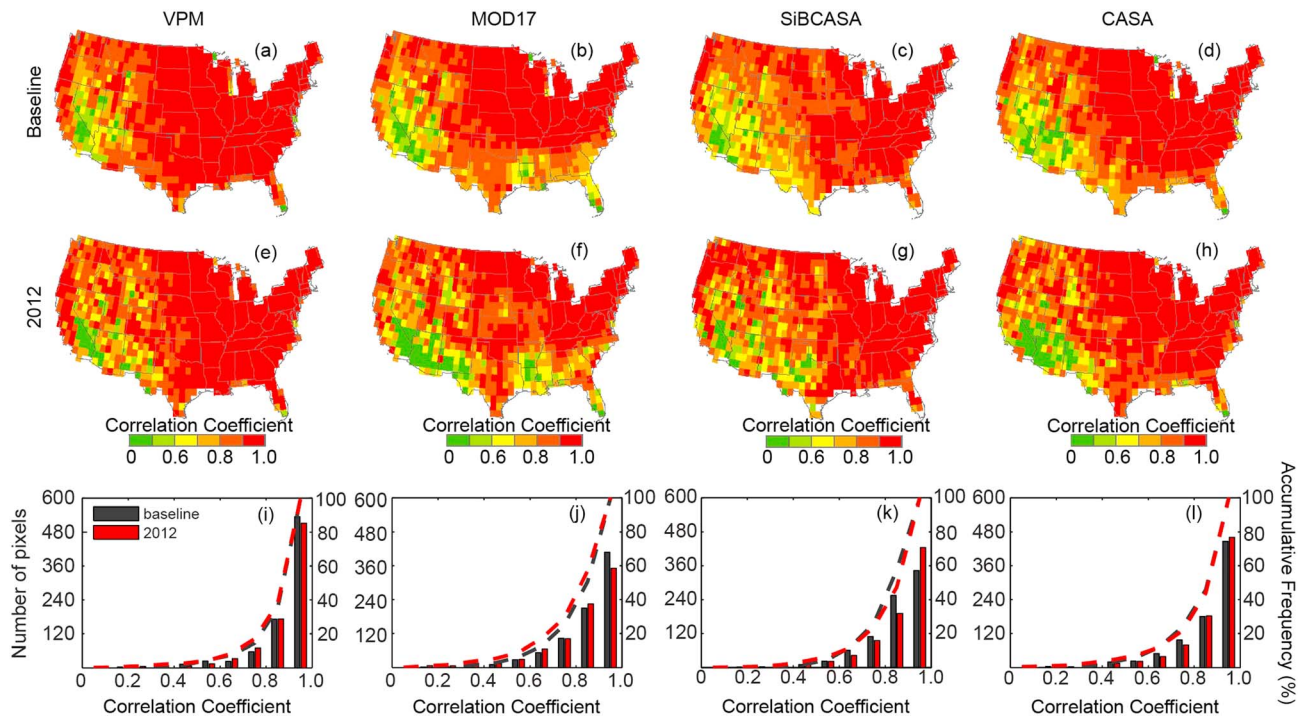


Figure 6. Spatial distribution of Pearson correlation coefficient between monthly solar-induced chlorophyll fluorescence and gross primary production products from VPM, MOD17, SiBCASA, and CASA for baseline year (the average of 2008, 2009, 2010, 2013, and 2014) and drought year 2012, and the corresponding frequency distribution (black and red bars) and accumulative frequency (black and red dashed lines) of the Pearson correlation coefficient for the four models in the baseline years and 2012. VPM = Vegetation Photosynthesis Model; CASA = Carnegie-Ames-Stanford Approach; SiBCASA = Simple Biosphere/CASA.

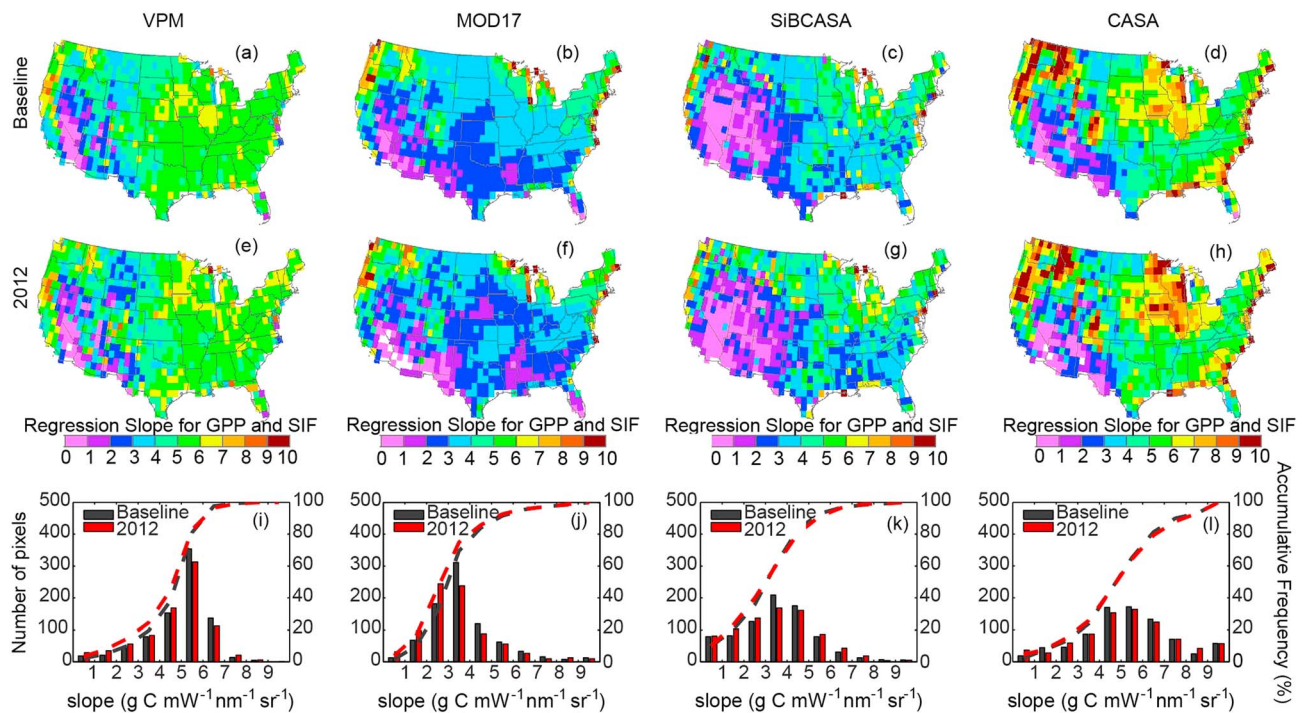


Figure 7. Spatial distribution of the regression slope between monthly SIF and GPP products from VPM, MOD17, SiBCASA, and CASA for the baseline year (the average of 2008, 2009, 2010, 2013, and 2014) and drought year 2012, and the corresponding frequency distribution (black and red bars) and accumulative frequency (black and red dashed lines) of the Pearson correlation coefficient for the four models in the baseline years and 2012. VPM = Vegetation Photosynthesis Model; CASA = Carnegie-Ames-Stanford Approach; SiBCASA = Simple Biosphere/CASA; GPP = gross primary production; SIF = solar-induced chlorophyll fluorescence.

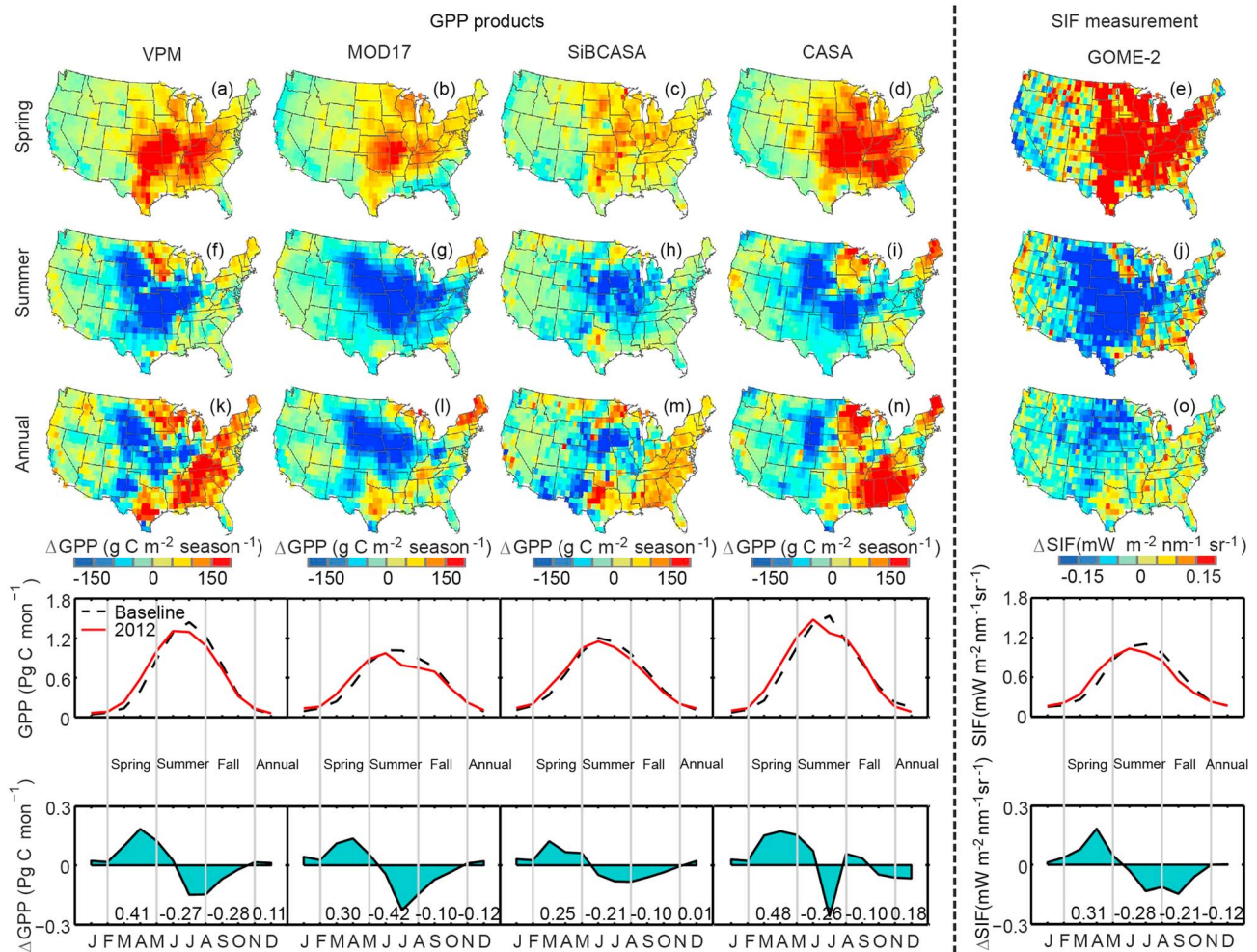


Figure 8. Spatial-temporal anomalies of GPP_{VPM} , GPP_{MOD17} , $GPP_{SiBCASA}$, GPP_{CASA} , and SIF during spring, summer, and annually across Contiguous United States in 2012 relative to the baseline (2008, 2009, 2010, 2013, and 2014). Seasonal cycle and anomaly of total monthly GPP_{VPM} , GPP_{MOD17} , $GPP_{SiBCASA}$, GPP_{CASA} , and SIF in 2012 relative to the baseline. Numbers shown in the last row of graphs are the anomaly of total GPP in spring (March–May), summer (June–August), fall (September–November), and the whole year (January to December). GPP = gross primary production; VPM = Vegetation Photosynthesis Model; CASA = Carnegie-Ames-Stanford Approach; SiBCASA = Simple Biosphere/CASA; GOME-2 = Global Ozone Monitoring Experiment-2; SIF = solar-induced chlorophyll fluorescence.

3.4. Impacts of Spring Warming and Summer Drought on GPP by Biomes in 2012

To quantify the impact of spring warming and summer drought on GPP across biomes, we calculated total GPP from the four models for the four main biomes. In the spring of 2012, all four models showed increased GPP for the four biomes (Figure 10 and Table 3), and the nonforest experienced a stronger increase in GPP than forest. In the four models, CASA showed a larger increase in GPP in the spring than other three models in the four biomes, while SiBCASA showed the lowest increase in GPP over most biomes. For the drought summer, all four models showed strong decreases in GPP, and the grassland and cropland experienced the strongest decrease, followed by other biomes. Among the four models, MOD17 showed the largest decrease in GPP in the summer, while SiBCASA showed the least decrease. For the entire year, grassland and cropland experienced a decrease in GPP, while forest and other biomes experienced an increase or no change.

4. Discussion

4.1. Improving GPP Estimates of C_3 and C_4 Croplands

Accurate estimation of cropland GPP is important for food production and security. The MOD17 GPP data products have been widely used for crop studies (Guan et al., 2016; Xin et al., 2015). However, several

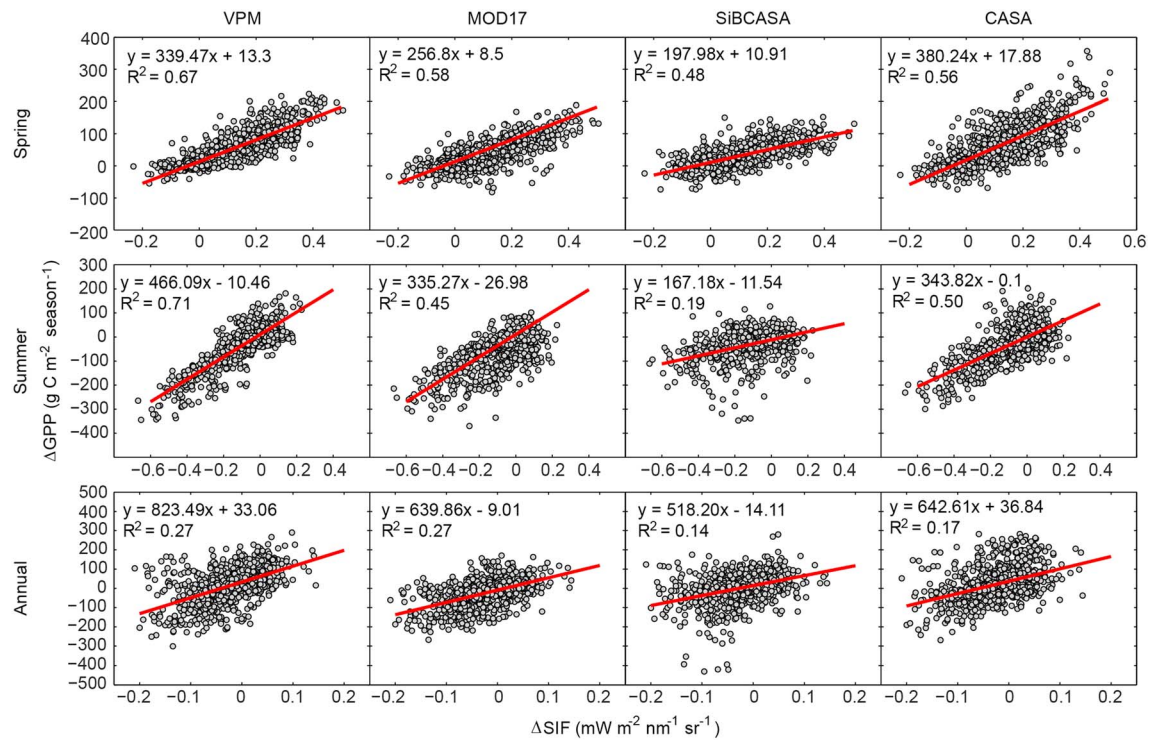


Figure 9. Correlation between the anomaly of seasonal/annual GPP from GPP models (VPM, MOD17, SiBCASA, and CASA) and the anomaly of seasonal/annual mean SIF from Global Ozone Monitoring Experiment-2 across Contiguous United States during the baseline years (the average of 2008, 2009, 2010, 2013, and 2014) and drought year 2012 (all of the correlations are significant with $p < 0.001$). GPP = gross primary production; VPM = Vegetation Photosynthesis Model; CASA = Carnegie-Ames-Stanford Approach; SiBCASA = Simple Biosphere/CASA; SIF = solar-induced chlorophyll fluorescence.

studies have reported that the MOD17 data product substantially underestimates GPP in croplands. One reason is that ϵ_{max} for croplands in the MOD17 model is too low (~ 1.04 g-C-MJ $^{-1}$; Turner et al., 2006; Wagle et al., 2016; Xin et al., 2015). Site-level studies have indicated that the typical ϵ_{max} for C₃ crops range from 1.43 to 1.96 g-C-MJ $^{-1}$ (T. Chen et al., 2011; Kalfas et al., 2011; Yuan et al., 2015) and ϵ_{max} for C₄ crops range from 2.25 to 4.06 g-C-MJ $^{-1}$ (Xin et al., 2015; Yuan et al., 2015). Several model comparison studies have also showed that both process-based GPP models and LUE models have poor performance when estimating GPP in croplands (Schaefer et al., 2012; Verma et al., 2014). Recently, Guanter et al. (2014) used GOME-2 SIF to estimate GPP in croplands using the linear relationship between SIF and tower-based GPP at flux tower sites, and they found these SIF-based GPP estimates in croplands were 50–60% higher than GPP estimates from the ecosystem models over the U.S. Corn Belt. In this study, our ϵ_{max} values for C₃ croplands (1.80 g-C-MJ $^{-1}$) and C₄ croplands (2.7 g-C-MJ $^{-1}$) were based on previous site-level studies (Li et al., 2013;

Table 2

The Anomaly of Total GPP Between 2012 and the Baseline (the Average of 2008, 2009, 2010, 2013, and 2014) in Spring (March–May), Summer (June–August), Fall (September–November), and the Whole Year

Anomaly of GPP (Pg C)	VPM	MODIS	CASA	SiBCASA	Anomaly of SIF (mW·m $^{-2}$ ·nm $^{-1}$ ·sr $^{-1}$)
Spring	0.41 ± 0.04	0.30 ± 0.03	0.48 ± 0.05	0.25 ± 0.03	0.31 ± 0.05
Summer	−0.27 ± 0.05	−0.42 ± 0.02	−0.26 ± 0.06	−0.21 ± 0.04	−0.28 ± 0.05
Annual	0.11 ± 0.08	−0.12 ± 0.02	0.18 ± 0.10	0.01 ± 0.08	−0.12 ± 0.10

Note. The uncertainty range of the anomaly was calculated as the standard deviation of the anomaly between 2012 and different baselines. We randomly chose at least 3 years from the year 2008, 2009, 2010, 2013, and 2014 to calculate the baseline, so there are 16 options (C₃³ + C₃⁴ + C₃⁵). GPP = gross primary production; VPM = Vegetation Photosynthesis Model; MODIS = Moderate Resolution Imaging Spectroradiometer; CASA = Carnegie-Ames-Stanford Approach; SiBCASA = Simple Biosphere/CASA; SIF = solar-induced chlorophyll fluorescence.

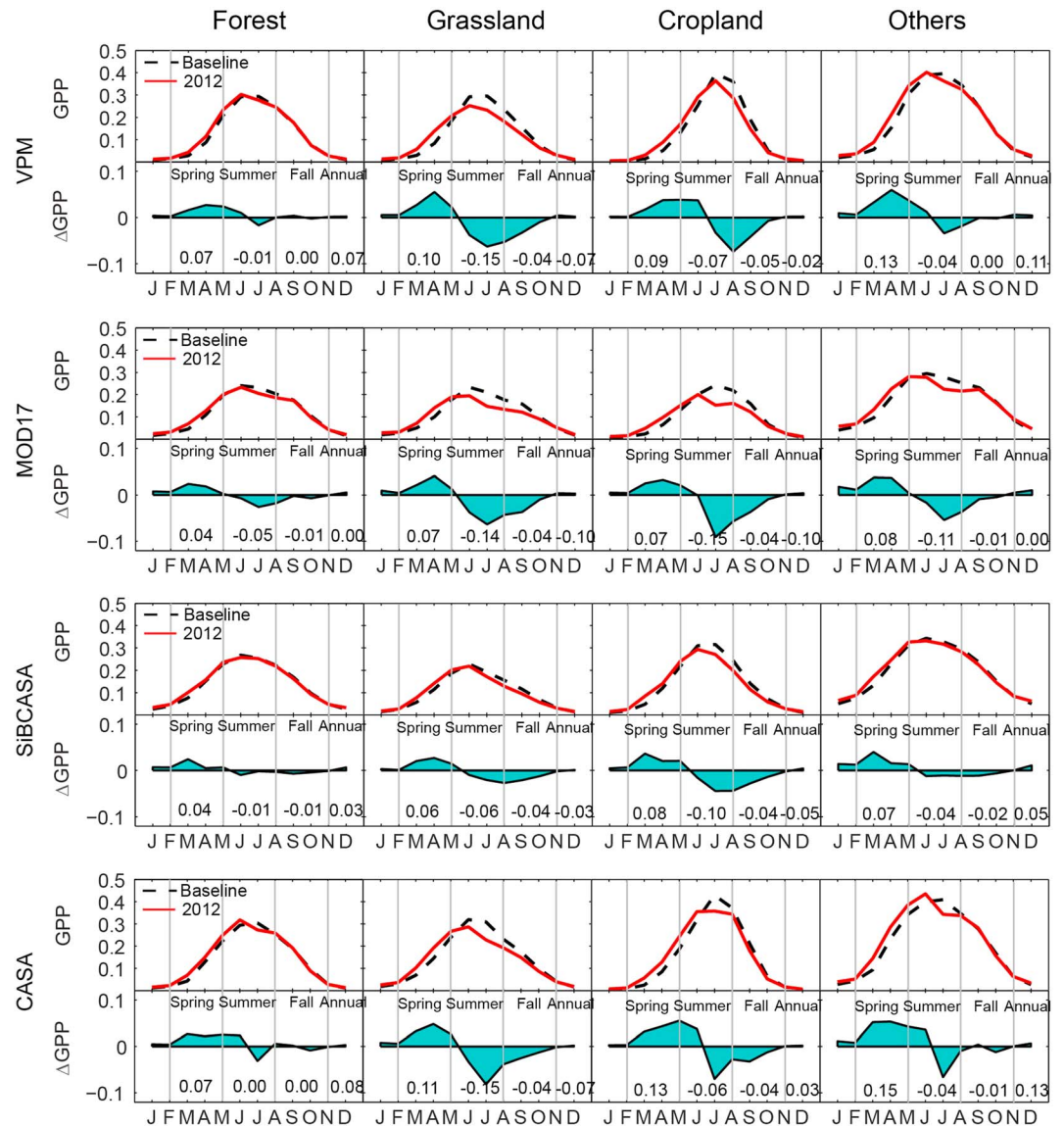


Figure 10. Seasonal cycle and anomaly of total monthly GPP_{VPM} , $GPP_{SiBCASA}$, GPP_{CASA} , and GPP_{MOD17} in forest, grassland, cropland and others. Numbers shown in the bottom panel in each row are the anomalies of total GPP for each biome in spring (March–May), summer (June–August), fall (September–November), and the whole year. CASA = Carnegie-Ames-Stanford Approach; SiBCASA = Simple Biosphere/CASA; VPM = Vegetation Photosynthesis Model; GPP = gross primary production.

Xin et al., 2015). The improved ability of VPM to capture the seasonal dynamics and interannual variability of croplands was partly attributed to more appropriate choices of ϵ_{max} values.

Another reason for the large error in estimating cropland GPP by the MOD17 and other models can be attributed to the fact that we have very limited knowledge on the spatial distribution of the C_3 and C_4 croplands within individual 500-m MODIS pixels and their temporal dynamics over years (Reeves et al., 2005; Still et al., 2003; Wang et al., 2013). However, in this study we used the fine-resolution, annual CDL cropland maps. The results demonstrated the potential of annual C_3/C_4 cropland maps at high spatial resolution to improve cropland GPP estimates from the individual pixel to country-wide scales. Although there are several existing global C_3/C_4 maps, they are relatively coarse in spatial resolution and produced only for a specific year. An early study developed a static C_3/C_4 fraction map with a spatial resolution of $1^\circ \times 1^\circ$ by defining the favorable climate zones for C_3/C_4 and combining the global spatial distribution of crop fractions and national harvest area

Table 3
The Anomaly of Total GPP Estimates From VPM, MOD17, SiBCASA, and CASA for Different Biomes Between 2012 and the Baseline (the Average of 2008, 2009, 2010, 2013, and 2014) in Spring (March–May), Summer (June–August), Fall (September–November), and the Whole Year

Anomaly of GPP (Pg C)		Spring	Summer	Fall	Annual
VPM	Forest	0.07	−0.01	0.00	0.07
	Grassland	0.10	−0.15	−0.04	−0.07
	Cropland	0.09	−0.07	−0.05	−0.02
	Others	0.13	−0.04	0.00	0.11
MOD17	Forest	0.04	−0.05	−0.01	0.00
	Grassland	0.07	−0.14	−0.04	−0.10
	Cropland	0.08	−0.15	−0.04	−0.10
SiBCASA	Others	0.08	−0.11	−0.01	0.00
	Forest	0.04	−0.01	−0.01	0.03
	Grassland	0.06	−0.06	−0.04	−0.03
	Cropland	0.08	−0.10	−0.04	−0.05
CASA	Others	0.07	−0.04	−0.02	0.05
	Forest	0.07	0.00	−0.01	0.08
	Grassland	0.11	−0.15	−0.04	−0.07
	Cropland	0.13	−0.06	−0.04	0.03
	Others	0.15	−0.04	−0.01	0.13

Note. Forest: evergreen needleleaf forest, evergreen broadleaf forest, deciduous broadleaf forest, deciduous needleleaf forest, mixed forest; Grassland: grassland; Cropland: cropland; Others: closed shrublands, open shrublands, savannahs, woody savannahs, permanent wetlands, cropland/natural vegetation mosaics. GPP = gross primary production; VPM = Vegetation Photosynthesis Model; CASA = Carnegie-Ames-Stanford Approach; SiBCASA = Simple Biosphere/CASA.

data for major crop types (Still et al., 2003). Another study developed a global distribution map of croplands and pastures at a 5 by 5 min (~10 km) spatial resolution in 2000 by combining agricultural inventory data and satellite-derived land cover data (Ramankutty et al., 2008). Recently, several studies made very limited progress in mapping C₃ and C₄ plants (both croplands and grasses) when using remote sensing data and simple algorithms (Foody & Dash, 2007; Wang et al., 2013). The development of CDL data sets include the use of satellite-based imagery, supervised image classification methodology, and numerous high-quality ground truth data collected to help determine the multispectral rules from time-series imagery that best predicted the land cover category. For grasslands, it was reported that there was a strong linear relationship between the percentage of C₃ grass and the season-long cumulative vegetation index (Foody & Dash, 2007). These phenological features and time-series MODIS data were used to classify C₃ and C₄ grasslands in the Great Plains (Wang et al., 2013). Given the importance of C₃ and C₄ plant function types in estimating GPP, it is important for the remote sensing community to increase its effort in mapping C₃ and C₄ croplands and grasslands at site, regional, and global scales.

4.2. The Timing and Location of Climate Extremes and Their Impacts on Terrestrial Ecosystems

Climate extremes such as heatwaves and droughts can reduce vegetative growth, trigger large-scale tree mortality, and turn terrestrial ecosystems from carbon sinks into sources (Ciais et al., 2005; Yuan et al., 2016). The warm spring and hot and dry summer in 2012 over CONUS offered a

unique opportunity to investigate several major questions on the impacts of climate extremes on terrestrial carbon cycle at the regional and continental scales (He et al., 2018; Sippel et al., 2016; Wolf et al., 2016). Many studies have reported that terrestrial ecosystems in CONUS have served as carbon sinks in recent decades (Hurt et al., 2002; Pacala et al., 2001), ranging from 0.30 to 0.58 pg C per year during the 1980s and 1990s, which accounts for 30% of fossil-fuel emissions from the United States. Wolf et al. (2016) analyzed MOD17 GPP data and NEP data from CTE2014 during 2001–2012 and reported that the increase of NEP in the spring compensated for the loss of NEP in the summer, which resulted in a small carbon sink (0.11 pg C per year in 2012) for CONUS. This result suggests the importance of assessing the impacts of climate extremes, which depend on timing, duration, and location, on terrestrial carbon budgets at the annual and continental scales (Sippel et al., 2017; von Buttlar et al., 2017).

Wolf et al. (2016) analyzed MOD17 GPP data in 2001–2012 and reported that GPP loss in summer in 2012 over CONUS was twice as large as the increase in GPP in the spring of 2012, resulting in a large annual loss of GPP (−0.38 pg C). Though we used a different baseline, our analysis of MOD17 GPP data in 2008–2014 also shows that the decrease in GPP in the summer of 2012 was substantially larger than the increase in GPP in the spring of 2012, resulting in large annual loss of GPP (−0.12 pg C; Figure 8). However, the results from GPP_{VPM}, GPP_{SiBCASA}, and GPP_{CASA} showed that the GPP increase in the spring is close or slightly larger than GPP loss in the summer of 2012, the annual GPP anomaly ranging from 0.01 (GPP_{SiBCASA}), to 0.11 (GPP_{VPM}), to 0.18 pg C (GPP_{CASA}), while the GOME-2 SIF anomaly showed a decrease in 2012 (Figure 7). The differences in modeling GPP responses to spring warming and summer drought among these four models are likely to affect our understanding of the responses of ER to spring warming and summer drought. As NEP is the sum of GPP (carbon gains) and ER (carbon losses), the large decrease in GPP (e.g., −0.38 pg C per year in 2012, GPP_{MOD17}) from the previous study (Wolf et al., 2016) implied a slightly larger decrease in ER, which could then result in a small carbon sink (0.11 pg C per year in 2012). In addition, since CASA-GFED3 and SiBCASA-GFED4 are the biosphere models used by CarbonTracker (CT2014) and CarbonTracker Europe (CTE2014) to generate prior biosphere carbon fluxes, the spatial-temporal differences in GPP distribution, magnitude, and anomaly from these two models are likely to affect CarbonTracker and CarbonTracker Europe outputs. Previous studies have reported that atmospheric CO₂ inversions are sensitive to the land surface prior fluxes, especially at fine

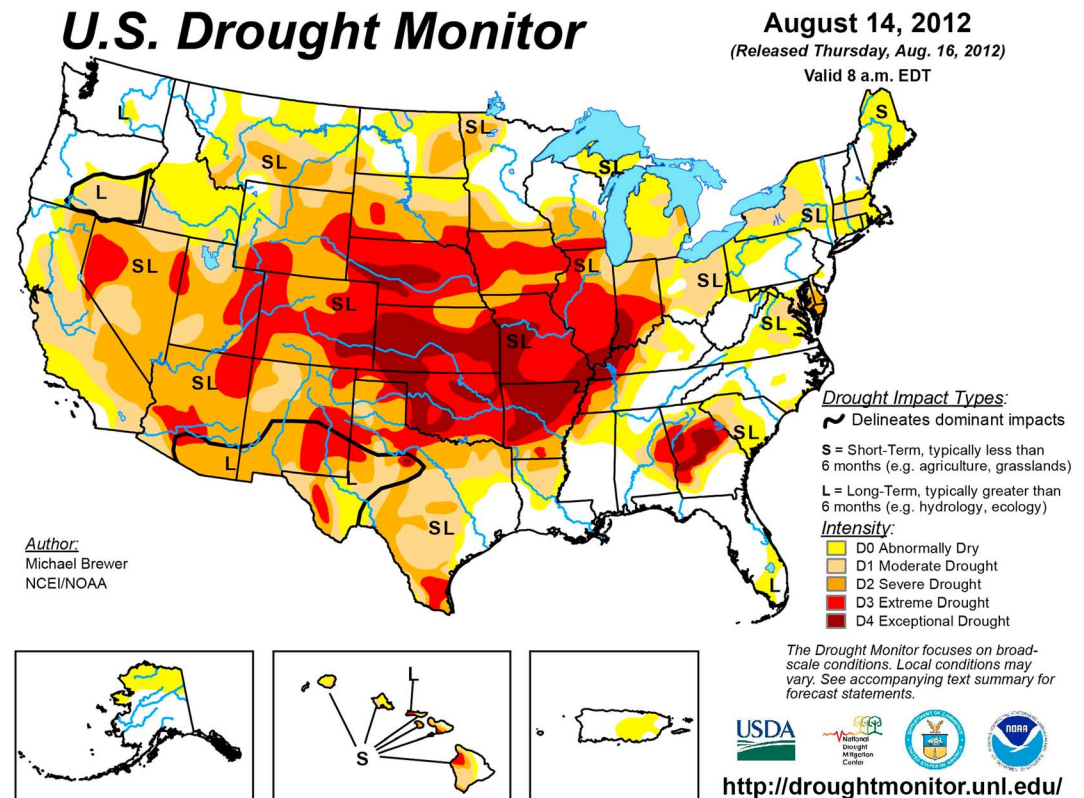


Figure 11. Drought-affected areas over Contiguous United States on 14 August 2012.

scales and the areas with sparse or no available observations (Peylin et al., 2013; Zhu et al., 2014). Therefore, methods to incorporate more reliable carbon flux estimates from atmospheric CO₂ inversions is critically needed for us to better understand the terrestrial carbon cycle.

4.3. Differential Responses to Climate Extremes Across Biomes

Numerous studies have reported the negative impacts of high temperature and droughts on vegetation productivity (Ciais et al., 2005; Welp et al., 2007; Wolf et al., 2016; Yuan et al., 2016). Short-term drought or heatwaves lead to stomatal closure, membrane damage, and disruption of photosynthetic enzyme activities, all of which reduce GPP. If plants experience continuous drought, they may respond to drought stress by structural or physiological adjustments such as decreased leaf area index, changes in the root-shoot ratio, or changes in leaf angle (Frank et al., 2015). But different species have adopted different strategies to deal with water stress. These strategies can be broadly classified as dehydration tolerance or dehydration avoidance (Bacelar et al., 2012). Plants with a dehydration tolerance strategy usually grow rapidly when water is available but will senesce and/or become dormant during drought. Plants with a dehydration avoidance strategy tend to grow more slowly and maintain greenness during drought by increasing water extraction from the soils and reducing water loss from transpiration. Our study showed that the impacts of spring warming and summer drought on the change in GPP varied across biomes (Figure 10). This change was not only due to the characteristics (timing, magnitude) of the heatwaves and drought at specific regions (Figure 11), but also species-specific plant drought responses and strategies (von Buttlar et al., 2017; Wolf et al., 2013). Our results show that grasslands experienced the largest reduction in GPP while forests had the largest increase. This difference may be explained by the observation that grasslands are drought sensitive and more susceptible to heatwaves and droughts as they have less accessibility to soil water (shallow roots) and higher turnover rates (Frank et al., 2015). Trees usually have deeper roots and better access to soil water, thus forests are considered to be less affected by heatwaves and drought (Frank et al., 2015; van der Molen et al., 2011; Zhang, Xiao, Zhou, et al., 2016). Grasslands occur in the most severe drought-affected areas, while most forests are in the northwestern and eastern part of CONUS, which were either not affected by the 2012 drought or were

classified as abnormally dry (D0) by the U.S. drought monitor (Figure 11). Cropland systems are different from natural systems by the frequent human intervention (e.g., irrigation or changing planting date). Consequently, the impacts of climate extremes on croplands are expected to be highly modulated by human management (Lobell et al., 2012; van der Velde et al., 2010). However, cropland over the Corn Belt, the most important crop area in the United States, is mainly rainfed (Leng et al., 2016), leading to a similar GPP response to drought for cropland and grasslands.

4.4. Uncertainties and Remaining Issues

The uncertainty of ecosystem models remains a challenge for carbon cycling research. Extreme climate events were found to dominate the global interannual variability of GPP (Zscheischler et al., 2014). At present, most ecological models do not accurately represent the responses of major ecosystem processes to climate extremes and do not accurately track the interannual variability of GPP (Reichstein et al., 2013). For example, previous studies indicated that improving GPP estimates for most models requires better representation of water stress effects on photosynthesis (Schaefer et al., 2012; Verma et al., 2014; Yuan et al., 2014). In this study, VPM, MOD17, and CASA are all light use efficiency models, but use different water regulation scalars. VPM uses a water-related vegetation index (LSWI) as the water constraint, MOD17 uses VPD, and CASA uses the evapotranspiration supply/demand ratio (actual evapotranspiration/potential evapotranspiration). LSWI is found to be a good indicator of soil moisture when taking all the biomes into consideration (Zhang et al., 2015). However, it may not work well for forested areas because of the lower spectral sensitivity to water stress (Sims et al., 2014). VPD represents the impacts of atmospheric dryness on vegetation photosynthesis because stomatal conductance changes with VPD. However, soil moisture also plays an important role in regulating GPP by affecting leaf cell turgor pressure or stomatal conductance, thereby directly affecting photosynthesis (Hashimoto et al., 2013; Leuning et al., 2005). The evapotranspiration ratio requires well simulated hydrologic fluxes in soils where additional information (e.g., soil texture, soil/rooting depth) is required. This information is usually not easy to collect and comes with uncertainties. Therefore, more effort is needed to quantify the model uncertainties and improve model structure.

Since SIF can be directly observed from space, has a very good relationship with GPP (Guanter et al., 2014; Wagle et al., 2016; Zhang, Xiao, Jin, et al., 2016), and is a good indicator of agricultural drought (Sun et al., 2015), we used SIF as a reference to which we compared the impacts of spring warming and summer droughts on vegetation photosynthesis. However, we acknowledge that GOME-2 SIF has some uncertainties, especially in the western part of CONUS (Figure 6) due to the relatively large signal-to-noise ratio (Zhang, Xiao, Jin, et al., 2016). SIF retrievals from recently launched satellites (OCO-2, Sentinel-5 Precursor, and FLEX-Fluorescence Explorer) with higher spatial resolutions and observations tailored for SIF may improve our understanding of the impacts of climate extremes on vegetation.

In this study, we only considered the impacts of climate extremes on terrestrial ecosystems within a year. However, droughts may affect terrestrial ecosystems across months or even years, depending upon plant functional types (Frank et al., 2015; von Buttlar et al., 2017). Extreme events could cause plant functional loss, changes in the community structure of ecosystems, increased wildfires, and pest and pathogen outbreaks, all which may necessitate a long recovery period (van der Molen et al., 2011). Further, species' response to climate extremes vary widely, and some impacts could persist long after extreme events (Rammig et al., 2014). Analysis of the responses of terrestrial ecosystems to climate extremes should be conducted over the next few years.

5. Conclusions

The spring warming and summer drought of 2012 across CONUS had substantial impacts on the terrestrial carbon cycle and offered a unique opportunity to investigate the responses of photosynthesis (GPP) and respiration processes at large scales. We presented an improved VPM model that incorporates C_3 and C_4 croplands and can better capture the seasonal dynamics and interannual variation of GPP than the MOD17 product when these models are compared to GPP_{EC} data from EC flux tower sites. Spatial-temporal comparisons among GOME-2 SIF, GPP_{MOD17} , and GPP_{VPM} products during 2008–2014 showed strong consistency between GOME-2 SIF and GPP_{VPM} data products. Anomaly analyses of (1) annual GPP from four models (VPM, MOD17, SiBCASA, and CASA) and (2) GOME-2 SIF data between the baseline years (2008, 2009, 2010, 2013, 2014) and drought year 2012 suggested that increased GPP during the warm spring compensated

for decreased GPP during the dry and hot summer, resulting in close to net neutral changes in annual GPP. The results from this study clearly highlight the importance of assessing the impacts of co-occurring climate extremes at seasonal and annual scales over large spatial domains. Our results demonstrate the need to further improve GPP models, which could increase the accuracy and reduce uncertainties in GPP estimates of terrestrial ecosystems.

Acknowledgments

This work used eddy covariance data acquired and shared by the FLUXNET community, including these networks: AmeriFlux, AfriFlux, AsiaFlux, CarboAfrica, CarboEuropeIP, CarboItaly, CarboMont, ChinaFlux, Fluxnet-Canada, GreenGrass, ICOS, KoFlux, LBA, NECC, OzFlux-TERN, TCOS-Siberia, and TERENO and USCCC. The FLUXNET eddy covariance data processing and harmonization was carried out by the ICOS Ecosystem Thematic Center, AmeriFlux Management Project and Fluxdata project of FLUXNET, with the support of CDIAC, and the OzFlux, ChinaFlux, and AsiaFlux offices. This study is partly supported by the research grants (Project No. 2013-69002-23146 and 2016-68002-24967) through the USDA National Institute for Food and Agriculture (NIFA), a research grant (IIA-1301789) from the US National Science Foundation EPSCoR program, and a research grant (Geostationary Carbon Cycle Observatory mission, 80LARC17C0001) from NASA. We acknowledge Ivar R. van der Velde for providing the SiBCASA-GFED4 simulations, the monthly $1^\circ \times 1^\circ$ SiBCASA-GFED4 GPP data over CONUS from 2008 to 2014 used is available at (https://github.com/xiaocuiwu/SiBCASA_GPP_monthly_CONUS.git). The CASA-GFED3 project (<https://nacp-files.nacarbon.org/nacp-kawa-01>) is supported by the North American Carbon Program. The VPM model code and the aggregated $1^\circ \times 1^\circ$ VPM GPP over CONUS from 2008 to 2014 are available at (https://github.com/xiaocuiwu/GPP_VPM_C3C4_CONUS.git).

References

- Bacelar, E. L. V. A., Moutinho-Pereira, J. M., Gonçalves, B. M. C., Brito, C. V. Q., Gomes-Laranjo, J., Ferreira, H. M. F., & Correia, C. M. (2012). Water use strategies of plants under drought conditions. In R. Arco (Ed.), *Plant responses to drought stress* (pp. 145–170). Berlin, Heidelberg: Springer. https://doi.org/10.1007/978-3-642-32653-0_6
- Baldocchi, D. D., Xu, L. K., & Kiang, N. (2004). How plant functional-type, weather, seasonal drought, and soil physical properties alter water and energy fluxes of an oak-grass savanna and an annual grassland. *Agricultural and Forest Meteorology*, *123*(1–2), 13–39. <https://doi.org/10.1016/j.agrformet.2003.11.006>
- Beer, C., Reichstein, M., Tomelleri, E., Ciais, P., Jung, M., Carvalhais, N., et al. (2010). Terrestrial gross carbon dioxide uptake: Global distribution and covariation with climate. *Science*, *329*(5993), 834–838. <https://doi.org/10.1126/science.1184984>
- Boryan, C., Yang, Z., Mueller, R., & Craig, M. (2011). Monitoring US agriculture: The US department of agriculture, national agricultural statistics service, cropland data layer program. *Geocarto International*, *26*(5), 341–358. <https://doi.org/10.1080/10106049.2011.562309>
- Cavanaugh, M. L., Kurc, S. A., & Scott, R. L. (2011). Evapotranspiration partitioning in semiarid shrubland ecosystems: A two-site evaluation of soil moisture control on transpiration. *Ecohydrology*, *4*(5), 671–681. <https://doi.org/10.1002/eco.157>
- Chen, J. M. (1996). Optically-based methods for measuring seasonal variation of leaf area index in boreal conifer stands. *Agricultural and Forest Meteorology*, *80*(2–4), 135–163. [https://doi.org/10.1016/0168-1923\(95\)02291-0](https://doi.org/10.1016/0168-1923(95)02291-0)
- Chen, T., van der Werf, G. R., Dolman, A. J., & Groenendijk, M. (2011). Evaluation of cropland maximum light use efficiency using eddy flux measurements in North America and Europe. *Geophysical Research Letters*, *38*, L14707. <https://doi.org/10.1029/2011GL047533>
- Chu, H. S., Chen, J. Q., Gottgens, J. F., Ouyang, Z. T., John, R., Czajkowski, K., & Becker, R. (2014). Net ecosystem methane and carbon dioxide exchanges in a Lake Erie coastal marsh and a nearby cropland. *Journal of Geophysical Research: Biogeosciences*, *119*, 722–740. <https://doi.org/10.1002/2013JG002520>
- Ciais, P., Reichstein, M., Viovy, N., Granier, A., Ogee, J., Allard, V., et al. (2005). Europe-wide reduction in primary productivity caused by the heat and drought in 2003. *Nature*, *437*(7058), 529–533. <https://doi.org/10.1038/nature03972>
- Collatz, G. J., Ribas-Carbo, M., & Berry, J. A. (1992). Coupled photosynthesis-stomatal conductance model for leaves of C4 plants. *Australian Journal of Plant Physiology*, *19*(5), 519–538. <https://doi.org/10.1071/PP9920519>
- Cook, B. D., Davis, K. J., Wang, W. G., Desai, A., Berger, B. W., Teclaw, R. M., et al. (2004). Carbon exchange and venting anomalies in an upland deciduous forest in northern Wisconsin, USA. *Agricultural and Forest Meteorology*, *126*(3–4), 271–295. <https://doi.org/10.1016/j.agrformet.2004.06.008>
- Disney, M., Lewis, P., & Saich, P. (2006). 3D modelling of forest canopy structure for remote sensing simulations in the optical and microwave domains. *Remote Sensing of Environment*, *100*(1), 114–132. <https://doi.org/10.1016/j.rse.2005.10.003>
- Dong, J. W., Xiao, X. M., Wagle, P., Zhang, G. L., Zhou, Y. T., Jin, C., et al. (2015). Comparison of four EVI-based models for estimating gross primary production of maize and soybean croplands and tallgrass prairie under severe drought. *Remote Sensing of Environment*, *162*, 154–168. <https://doi.org/10.1016/j.rse.2015.02.022>
- Doughty, R., Xiao, X., Wu, X., Zhang, Y., Bajgain, R., Zhou, Y., et al. (2018). Responses of gross primary production of grasslands and croplands under drought, pluvial, and irrigation conditions during 2010–2016, Oklahoma, USA. *Agricultural Water Management*, *204*, 47–59. <https://doi.org/10.1016/j.agwat.2018.04.001>
- Farquhar, G. D., Caemmerer, S. V., & Berry, J. A. (1980). A biochemical model of photosynthetic CO₂ assimilation in leaves of C₃ species. *Planta*, *149*(1), 78–90. <https://doi.org/10.1007/BF00386231>
- Fischer, M. L., Billesbach, D. P., Berry, J. A., Riley, W. J., & Torn, M. S. (2007). Spatiotemporal variations in growing season exchanges of CO₂, H₂O, and sensible heat in agricultural fields of the southern Great Plains. *Earth Interactions*, *11*(17), 1–21. <https://doi.org/10.1175/EI231.1>
- Foody, G. M., & Dash, J. (2007). Discriminating and mapping the C3 and C4 composition of grasslands in the northern Great Plains, USA. *Ecological Informatics*, *2*(2), 89–93. <https://doi.org/10.1016/j.ecoinf.2007.03.009>
- Frank, D., Reichstein, M., Bahn, M., Thonicke, K., Frank, D., Mahecha, M. D., et al. (2015). Effects of climate extremes on the terrestrial carbon cycle: Concepts, processes and potential future impacts. *Global Change Biology*, *21*(8), 2861–2880. <https://doi.org/10.1111/gcb.12916>
- Frankenberg, C., Fisher, J. B., Worden, J., Badgley, G., Saatchi, S. S., Lee, J.-E., et al. (2011). New global observations of the terrestrial carbon cycle from GOSAT: Patterns of plant fluorescence with gross primary productivity. *Geophysical Research Letters*, *38*, L17706. <https://doi.org/10.1029/2011GL048738>
- Friedl, M. A., Sulla-Menashe, D., Tan, B., Schneider, A., Ramankutty, N., Sibley, A., & Huang, X. (2010). MODIS collection 5 global land cover: Algorithm refinements and characterization of new datasets. *Remote Sensing of Environment*, *114*(1), 168–182. <https://doi.org/10.1016/j.rse.2009.08.016>
- Gough, C. M., Hardiman, B. S., Nave, L. E., Bohrer, G., Maurer, K. D., Vogel, C. S., et al. (2013). Sustained carbon uptake and storage following moderate disturbance in a Great Lakes forest. *Ecological Applications*, *23*(5), 1202–1215. <https://doi.org/10.1890/12-1554.1>
- Gough, C. M., Vogel, C. S., Schmid, H. P., Su, H. B., & Curtis, P. S. (2008). Multi-year convergence of biometric and meteorological estimates of forest carbon storage. *Agricultural and Forest Meteorology*, *148*(2), 158–170. <https://doi.org/10.1016/j.agrformet.2007.08.004>
- Guan, K., Berry, J. A., Zhang, Y., Joiner, J., Guanter, L., Badgley, G., & Lobell, D. B. (2016). Improving the monitoring of crop productivity using spaceborne solar-induced fluorescence. *Global Change Biology*, *22*(2), 716–726. <https://doi.org/10.1111/gcb.13136>
- Guanter, L., Zhang, Y., Jung, M., Joiner, J., Voigt, M., Berry, J. A., et al. (2014). Global and time-resolved monitoring of crop photosynthesis with chlorophyll fluorescence. *Proceedings of the National Academy of Sciences of the United States of America*, *111*(14), E1327–E1333. <https://doi.org/10.1073/pnas.1320008111>
- Hashimoto, H., Wang, W., Milesi, C., Xiong, J., Ganguly, S., Zhu, Z., & Nemani, R. (2013). Structural uncertainty in model-simulated trends of global gross primary production. *Remote Sensing*, *5*(3), 1258–1273. <https://doi.org/10.3390/rs5031258>
- Hatala, J. A., Detto, M., Sonntag, O., Deverel, S. J., Verfaillie, J., & Baldocchi, D. D. (2012). Greenhouse gas (CO₂, CH₄, H₂O) fluxes from drained and flooded agricultural peatlands in the Sacramento-San Joaquin Delta. *Agriculture Ecosystems & Environment*, *150*, 1–18. <https://doi.org/10.1016/j.agee.2012.01.009>

- He, W., Ju, W., Schwalm, C., Sippel, S., Wu, X., He, Q., et al. (2018). Terrestrial net carbon uptake over North America in 2011 and 2012. *Journal of Geophysical Research: Biogeosciences*, 123(7), 2053–2071. <https://doi.org/10.1029/2018JG004520>
- Hilker, T., Lyapustin, A. I., Tucker, C. J., Hall, F. G., Myneni, R. B., Wang, Y. J., et al. (2014). Vegetation dynamics and rainfall sensitivity of the Amazon. *Proceedings of the National Academy of Sciences of the United States of America*, 111(45), 16,041–16,046. <https://doi.org/10.1073/pnas.1404870111>
- Hilton, T. W., Whelan, M. E., Zumkehr, A., Kulkarni, S., Berry, J. A., Baker, I. T., et al. (2017). Peak growing season gross uptake of carbon in North America is largest in the Midwest USA. *Nature Climate Change*, 7(6), 450–454. <https://doi.org/10.1038/nclimate3272>
- Hilton, T. W., Zumkehr, A., Kulkarni, S., Berry, J., Whelan, M. E., & Campbell, J. E. (2015). Large variability in ecosystem models explains uncertainty in a critical parameter for quantifying GPP with carbonyl sulphide. *Tellus Series B-Chemical and Physical Meteorology*, 67(1), 26329. <https://doi.org/10.3402/tellusb.v67.26329>
- Hoerling, M., Eischeid, J., Kumar, A., Leung, R., Mariotti, A., Mo, K., et al. (2014). Causes and predictability of the 2012 Great Plains drought. *Bulletin of the American Meteorological Society*, 95(2), 269–282. <https://doi.org/10.1175/BAMS-D-13-00055.1>
- Huete, A. R., Liu, H. Q., Batchily, K., & vanLeeuwen, W. (1997). A comparison of vegetation indices global set of TM images for EOS-MODIS. *Remote Sensing of Environment*, 59(3), 440–451. [https://doi.org/10.1016/S0034-4257\(96\)00112-5](https://doi.org/10.1016/S0034-4257(96)00112-5)
- Hurt, G. C., Pacala, S. W., Moorcroft, P. R., Caspersen, J., Shevliakova, E., Houghton, R. A., & Moore, B. III (2002). Projecting the future of the U.S. carbon sink. *Proceedings of the National Academy of Sciences of the United States of America*, 99(3), 1389–1394. <https://doi.org/10.1073/pnas.012249999>
- Jin, C., Xiao, X., Merbold, L., Arneeth, A., Veenendaal, E., & Kutsch, W. L. (2013). Phenology and gross primary production of two dominant savanna woodland ecosystems in southern Africa. *Remote Sensing of Environment*, 135, 189–201. <https://doi.org/10.1016/j.rse.2013.03.033>
- Jin, C., Xiao, X. M., Wagler, P., Griffis, T., Dong, J. W., Wu, C. Y., et al. (2015). Effects of in-situ and reanalysis climate data on estimation of cropland gross primary production using the vegetation photosynthesis model. *Agricultural and Forest Meteorology*, 213, 240–250. <https://doi.org/10.1016/j.agrformet.2015.07.003>
- Joiner, J., Guanter, L., Lindstrot, R., Voigt, M., Vasilkov, A. P., Middleton, E. M., et al. (2013). Global monitoring of terrestrial chlorophyll fluorescence from moderate-spectral-resolution near-infrared satellite measurements: Methodology, simulations, and application to GOME-2. *Atmospheric Measurement Techniques*, 6(10), 2803–2823. <https://doi.org/10.5194/amt-6-2803-2013>
- Kalfas, J. L., Xiao, X., Vanegas, D. X., Verma, S. B., & Suyker, A. E. (2011). Modeling gross primary production of irrigated and rain-fed maize using MODIS imagery and CO₂ flux tower data. *Agricultural and Forest Meteorology*, 151(12), 1514–1528. <https://doi.org/10.1016/j.agrformet.2011.06.007>
- Knutson, T. R., Zeng, F., & Wittenberg, A. T. (2013). The extreme March–May 2012 warm anomaly over the eastern United States: Global context and multimodel trend analysis. *Bulletin of the American Meteorological Society*, 94, S13–S17.
- Lasslop, G., Reichstein, M., Papale, D., Richardson, A. D., Arneeth, A., Barr, A., et al. (2010). Separation of net ecosystem exchange into assimilation and respiration using a light response curve approach: Critical issues and global evaluation. *Global Change Biology*, 16(1), 187–208. <https://doi.org/10.1111/j.1365-2486.2009.02041.x>
- Law, B. E., Turner, D., Campbell, J., Sun, O. J., Van Tuyl, S., Ritts, W. D., & Cohen, W. B. (2004). Disturbance and climate effects on carbon stocks and fluxes across Western Oregon USA. *Global Change Biology*, 10(9), 1429–1444. <https://doi.org/10.1111/j.1365-2486.2004.00822.x>
- Law, B. E., Williams, M., Anthoni, P. M., Baldocchi, D., & Unsworth, M. H. (2000). Measuring and modelling seasonal variation of carbon dioxide and water vapour exchange of a *Pinus ponderosa* forest subject to soil water deficit. *Global Change Biology*, 6(6), 613–630. <https://doi.org/10.1046/j.1365-2486.2000.00339.x>
- Le Quéré, C., Raupach, M. R., Canadell, J. G., Marland, G., Bopp, L., Ciais, P., et al. (2009). Trends in the sources and sinks of carbon dioxide. *Nature Geoscience*, 2(12), 831–836. <https://doi.org/10.1038/ngeo689>
- Leng, G. Y., Zhang, X. S., Huang, M. Y., Yang, Q. C., Rafique, R., Asrar, G. R., & Leung, L. R. (2016). Simulating county-level crop yields in the conterminous United States using the community land model: The effects of optimizing irrigation and fertilization. *Journal of Advances in Modeling Earth Systems*, 8(4), 1912–1931. <https://doi.org/10.1002/2016MS000645>
- Leuning, R., Cleugh, H. A., Zegelin, S. J., & Hughes, D. (2005). Carbon and water fluxes over a temperate Eucalyptus forest and a tropical wet/dry savanna in Australia: Measurements and comparison with MODIS remote sensing estimates. *Agricultural and Forest Meteorology*, 129(3–4), 151–173. <https://doi.org/10.1016/j.agrformet.2004.12.004>
- Li, X. L., Liang, S. L., Yu, G. R., Yuan, W. P., Cheng, X., Xia, J. Z., et al. (2013). Estimation of gross primary production over the terrestrial ecosystems in China. *Ecological Modelling*, 261, 80–92.
- Lobell, D. B., Hicke, J. A., Asner, G. P., Field, C., Tucker, C., & Los, S. (2002). Satellite estimates of productivity and light use efficiency in United States agriculture, 1982–98. *Global Change Biology*, 8(8), 722–735. <https://doi.org/10.1046/j.1365-2486.2002.00503.x>
- Lobell, D. B., Sibley, A., & Ivan Ortiz-Monasterio, J. (2012). Extreme heat effects on wheat senescence in India. *Nature Climate Change*, 2(3), 186–189. <https://doi.org/10.1038/nclimate1356>
- Ma, S., Baldocchi, D. D., Xu, L., & Hehn, T. (2007). Inter-annual variability in carbon dioxide exchange of an oak/grass savanna and open grassland in California. *Agricultural and Forest Meteorology*, 147(3–4), 157–171. <https://doi.org/10.1016/j.agrformet.2007.07.008>
- Matamala, R., Jastrow, J. D., Miller, R. M., & Garten, C. T. (2008). Temporal changes in C and N stocks of restored prairie: Implications for C sequestration strategies. *Ecological Applications*, 18(6), 1470–1488. <https://doi.org/10.1890/07-1609.1>
- Monson, R. K., Turnipseed, A. A., Sparks, J. P., Harley, P. C., Scott-Denton, L. E., Sparks, K., & Huxman, T. E. (2002). Carbon sequestration in a high-elevation, subalpine forest. *Global Change Biology*, 8(5), 459–478.
- Monteith, J. L. (1972). Solar-radiation and productivity in tropical ecosystems. *Journal of Applied Ecology*, 9(3), 747–766. <https://doi.org/10.2307/2401901>
- Monteith, J. L. (1977). Climate and efficiency of crop production in Britain. *Philosophical Transactions of the Royal Society of London. Series B, Biological Sciences*, 281(980), 277–294. <https://doi.org/10.1098/rstb.1977.0140>
- Ollinger, S. V. (2011). Sources of variability in canopy reflectance and the convergent properties of plants. *New Phytologist*, 189(2), 375–394. <https://doi.org/10.1111/j.1469-8137.2010.03536.x>
- Pacala, S., Hurtt, G., Baker, D. B., & Peylin, P. (2001). Consistent land- and atmosphere-based US carbon sink estimates. *Science*, 292(5525), 2316–2320. <https://doi.org/10.1126/science.1057320>
- Pan, Y. D., & Schimel, D. (2016). Biogeochemistry: Synergy of a warm spring and dry summer. *Nature*, 534(7608), 483–484. <https://doi.org/10.1038/nature18450>
- Parazoo, N. C., Barnes, E., Worden, J., Harper, A. B., Bowman, K. B., Frankenberg, C., et al. (2015). Influence of ENSO and the NAO on terrestrial carbon uptake in the Texas-northern Mexico region. *Global Biogeochemical Cycles*, 29(8), 1247–1265. <https://doi.org/10.1002/2015GB005125>

- Peters, W., Jacobson, A. R., Sweeney, C., Andrews, A. E., Conway, T. J., Masarie, K., et al. (2007). An atmospheric perspective on North American carbon dioxide exchange: CarbonTracker. *Proceedings of the National Academy of Sciences of the United States of America*, *104*(48), 18,925–18,930. <https://doi.org/10.1073/pnas.0708986104>
- Peylin, P., Law, R. M., Gurney, K. R., Chevallier, F., Jacobson, A. R., Maki, T., et al. (2013). Global atmospheric carbon budget: Results from an ensemble of atmospheric CO₂ inversions. *Biogeosciences*, *10*(10), 6699–6720. <https://doi.org/10.5194/bg-10-6699-2013>
- Porcar-Castell, A., Tyystjarvi, E., Atherton, J., van der Tol, C., Flexas, J., Pfundel, E. E., et al. (2014). Linking chlorophyll a fluorescence to photosynthesis for remote sensing applications: Mechanisms and challenges. *Journal of Experimental Botany*, *65*(15), 4065–4095. <https://doi.org/10.1093/jxb/eru191>
- Potter, C., Klooster, S., Genovesi, V., Hiatt, C., Boriah, S., Kumar, V., et al. (2012). Terrestrial ecosystem carbon fluxes predicted from MODIS satellite data and large-scale disturbance modeling. *International Journal of Geosciences*, *03*(03), 469–479. <https://doi.org/10.4236/ijg.2012.33050>
- Potter, C., Randerson, J. T., Field, C., Matson, P., Vitousek, P., Mooney, H., & Klooster, S. (1993). Terrestrial ecosystem production: A process model based on global satellite and surface data. *Global Biogeochemical Cycles*, *7*(4), 811–841. <https://doi.org/10.1029/93GB02725>
- Ramankutty, N., Evan, A. T., Monfreda, C., & Foley, J. A. (2008). Farming the planet: 1. Geographic distribution of global agricultural lands in the year 2000. *Global Biogeochemical Cycles*, *22*, GB1003. <https://doi.org/10.1029/2007GB002953>
- Rammig, A., Wiedermann, M., Donges, J. F., Babst, F., von Bloh, W., Frank, D., et al. (2014). Tree-ring responses to extreme climate events as benchmarks for terrestrial dynamic vegetation models. *Biogeosciences Discussions*, *11*(2), 2537–2568. <https://doi.org/10.5194/bgd-11-2537-2014>
- Randerson, J. T., Thompson, M. V., Malmstrom, C. M., Field, C. B., & Fung, I. Y. (1996). Substrate limitations for heterotrophs: Implications for models that estimate the seasonal cycle of atmospheric CO₂. *Global Biogeochemical Cycles*, *10*(4), 585–602. <https://doi.org/10.1029/96GB01981>
- Reeves, M. C., Zhao, M., & Running, S. W. (2005). Usefulness and limits of MODIS GPP for estimating wheat yield. *International Journal of Remote Sensing*, *26*(7), 1403–1421. <https://doi.org/10.1080/01431160512331326567>
- Reichstein, M., Bahn, M., Ciais, P., Frank, D., Mahecha, M. D., Seneviratna, S. I., et al. (2013). Climate extremes and the carbon cycle. *Nature*, *500*(7462), 287–295. <https://doi.org/10.1038/nature12350>
- Reichstein, M., Ciais, P., Papale, D., Valentini, R., Running, S., Viivy, N., et al. (2007). Reduction of ecosystem productivity and respiration during the European summer 2003 climate anomaly: A joint flux tower, remote sensing and modelling analysis. *Global Change Biology*, *13*(3), 634–651. <https://doi.org/10.1111/j.1365-2486.2006.01224.x>
- Reichstein, M., Falge, E., Baldocchi, D., Papale, D., Aubinet, M., Berbigier, P., et al. (2005). On the separation of net ecosystem exchange into assimilation and ecosystem respiration: Review and improved algorithm. *Global Change Biology*, *11*(9), 1424–1439. <https://doi.org/10.1111/j.1365-2486.2005.001002.x>
- Rippey, B. R. (2015). The US drought of 2012. *Weather and Climate Extremes*, *10*(Part A), 57–64. <https://doi.org/10.1016/j.wace.2015.10.004>
- Running, S., Nemani, R., Heinsch, F. A., Zhao, M., Reeves, M., & Hashimoto, H. (2004). A contiguous satellite-derived measure of global terrestrial primary production. *Bioscience*, *54*(6), 547–560. [https://doi.org/10.1641/0006-3568\(2004\)054\[0547:ACSMOG\]2.0.CO;2](https://doi.org/10.1641/0006-3568(2004)054[0547:ACSMOG]2.0.CO;2)
- Schaefer, K., Collatz, G. J., Tans, P., Denning, A. S., Baker, I., Berry, J., et al. (2008). Combined simple biosphere/Carnegie-Ames-Stanford approach terrestrial carbon cycle model. *Journal of Geophysical Research*, *113*, G03034. <https://doi.org/10.1029/2007JG000603>
- Schaefer, K., Schwalm, C. R., Williams, C., Arain, M. A., Barr, A., Chen, J. M., et al. (2012). A model-data comparison of gross primary productivity: Results from the North American Carbon Program site synthesis. *Journal of Geophysical Research*, *113*, G03034. <https://doi.org/10.1029/2007JG000603>
- Schmid, H. P., Grimmond, S. B., Cropley, F., Offerle, B., & Su, H. (2000). Measurements of CO₂ and energy fluxes over a mixed hardwood forest in the mid-western United States. *Agricultural and Forest Meteorology*, *103*(4), 357–374. [https://doi.org/10.1016/S0168-1923\(00\)00140-4](https://doi.org/10.1016/S0168-1923(00)00140-4)
- Schwalm, C. R., Williams, C. A., Schaefer, K., Anderson, R., Arain, M. A., Baker, I., et al. (2010). A model-data intercomparison of CO₂ exchange across North America: Results from the North American Carbon Program site synthesis. *Journal of Geophysical Research*, *115*, G00H05. <https://doi.org/10.1029/2009JG001229>
- Scott, R. L., Biederman, J. A., Hamerlynck, E. P., & Barron-Gafford, G. A. (2015). The carbon balance pivot point of southwestern US semiarid ecosystems: Insights from the 21st century drought. *Journal of Geophysical Research: Biogeosciences*, *120*, 2612–2624. <https://doi.org/10.1002/2015JG003181>
- Scott, R. L., Hamerlynck, E. P., Jenerette, G. D., Moran, M. S., & Barron-Gafford, G. A. (2010). Carbon dioxide exchange in a semidesert grassland through drought-induced vegetation change. *Journal of Geophysical Research*, *115*, G03026. <https://doi.org/10.1029/2010JG001348>
- Scott, R. L., Jenerette, G. D., Potts, D. L., & Huxman, T. E. (2009). Effects of seasonal drought on net carbon dioxide exchange from a woody plant-encroached semiarid grassland. *Journal of Geophysical Research*, *114*, G04004. <https://doi.org/10.1029/2008JG000900>
- Sims, D. A., Brzostek, E. R., Rahman, A. F., Dragoni, D., & Phillips, R. P. (2014). An improved approach for remotely sensing water stress impacts on forest C uptake. *Global Change Biology*, *20*(9), 2856–2866. <https://doi.org/10.1111/gcb.12537>
- Sippel, S., Forkel, M., Rammig, A., Thonicke, K., Flach, M., Heimann, M., et al. (2017). Contrasting and interacting changes in simulated spring and summer carbon cycle extremes in European ecosystems. *Environmental Research Letters*, *12*(7), 075006. <https://doi.org/10.1088/1748-9326/aa7398>
- Sippel, S., Zscheischler, J., & Reichstein, M. (2016). Ecosystem impacts of climate extremes crucially depend on the timing. *Proceedings of the National Academy of Sciences of the United States of America*, *113*(21), 5768–5770. <https://doi.org/10.1073/pnas.1605667113>
- Still, C. J., Berry, J. A., Collatz, G. J., & DeFries, R. S. (2003). Global distribution of C₃ and C₄ vegetation: Carbon cycle implications. *Global Biogeochemical Cycles*, *17*, 1006. <https://doi.org/10.1029/2001GB001807>
- Sturtevant, C., Ruddell, B. L., Knox, S. H., Verfaillie, J., Matthes, J. H., Oikawa, P. Y., & Baldocchi, D. (2016). Identifying scale-emergent, nonlinear, asynchronous processes of wetland methane exchange. *Journal of Geophysical Research: Biogeosciences*, *121*, 188–204. <https://doi.org/10.1002/2015JG003054>
- Sun, Y., Frankenberg, C., Wood, J. D., Schimel, D. S., Jung, M., Guanter, L., et al. (2017). OCO-2 advances photosynthesis observation from space via solar-induced chlorophyll fluorescence. *Science*, *358*(6360), eaam5747. <https://doi.org/10.1126/science.aam5747>
- Sun, Y., Fu, R., Dickinson, R., Joiner, J., Frankenberg, C., Gu, L. H., et al. (2015). Drought onset mechanisms revealed by satellite solar-induced chlorophyll fluorescence: Insights from two contrasting extreme events. *Journal of Geophysical Research: Biogeosciences*, *120*, 2427–2440. <https://doi.org/10.1002/2015JG003150>
- Suyker, A. E., Verma, S. B., Burba, G. G., & Arkebauer, T. J. (2005). Gross primary production and ecosystem respiration of irrigated maize and irrigated soybean during a growing season. *Agricultural and Forest Meteorology*, *131*(3–4), 180–190. <https://doi.org/10.1016/j.agrformet.2005.05.007>
- Turner, D. P., Ritts, W. D., Cohen, W. B., Gower, S. T., Running, S. W., Zhao, M., et al. (2006). Evaluation of MODIS NPP and GPP products across multiple biomes. *Remote Sensing of Environment*, *102*(3–4), 282–292. <https://doi.org/10.1016/j.rse.2006.02.017>

- Urbanski, S., Barford, C., Wofsy, S., Kucharik, C., Pyle, E., Budney, J., et al. (2007). Factors controlling CO₂ exchange on timescales from hourly to decadal at Harvard Forest. *Journal of Geophysical Research*, *112*, G02020. <https://doi.org/10.1029/2006JG000293>
- van der Laan-Luijckx, I. T., van der Velde, I. R., van der Veen, E., Tsuruta, A., Stanislawska, K., Babenhausenerheide, A., et al. (2017). The CarbonTracker Data Assimilation Shell (CTDAS) v1.0: Implementation and global carbon balance 2001–2015. *Geoscientific Model Development*, *10*(7), 2785–2800. <https://doi.org/10.5194/gmd-10-2785-2017>
- van der Molen, M. K., Dolman, A. J., Ciais, P., Eglin, T., Gobron, N., Law, B. E., et al. (2011). Drought and ecosystem carbon cycling. *Agricultural and Forest Meteorology*, *151*(7), 765–773. <https://doi.org/10.1016/j.agrformet.2011.01.018>
- van der Velde, I. R., Miller, J. B., Schaefer, K., van der Werf, G. R., Krol, M. C., & Peters, W. (2014). Terrestrial cycling of 13CO₂ by photosynthesis, respiration, and biomass burning in SiBCASA. *Biogeosciences*, *11*(23), 6553–6571. <https://doi.org/10.5194/bg-11-6553-2014>
- van der Velde, M., Wriedt, G., & Bouraoui, F. (2010). Estimating irrigation use and effects on maize yield during the 2003 heatwave in France. *Agriculture, Ecosystems & Environment*, *135*(1–2), 90–97. <https://doi.org/10.1016/j.agee.2009.08.017>
- van der Werf, G. R., Randerson, J. T., Giglio, L., Collatz, G. J., Kasibhatla, P. S., & Arellano, A. F. (2006). Interannual variability in global biomass burning emissions from 1997 to 2004. *Atmospheric Chemistry and Physics*, *6*(11), 3423–3441. <https://doi.org/10.5194/acp-6-3423-2006>
- van der Werf, G. R., Randerson, J. T., Giglio, L., Collatz, G. J., Mu, M., Kasibhatla, P. S., et al. (2010). Global fire emissions and the contribution of deforestation, savanna, forest, agricultural, and peat fires (1997–2009). *Atmospheric Chemistry and Physics*, *10*(23), 11,707–11,735. <https://doi.org/10.5194/acp-10-11707-2010>
- van Gorsel, E., Del Pierre, N., Leuning, R., Black, A., Munger, J. W., Wofsy, S., et al. (2009). Estimating nocturnal ecosystem respiration from the vertical turbulent flux and change in storage of CO₂. *Agricultural and Forest Meteorology*, *149*(11), 1919–1930. <https://doi.org/10.1016/j.agrformet.2009.06.020>
- Verma, M., Friedl, M. A., Richardson, A. D., Kiely, G., Cescatti, A., Law, B. E., et al. (2014). Remote sensing of annual terrestrial gross primary productivity from MODIS: An assessment using the FLUXNET La Thuile data set. *Biogeosciences*, *11*(8), 2185–2200. <https://doi.org/10.5194/bg-11-2185-2014>
- von Buttler, J., Zscheischler, J., Rammig, A., Sippel, S., Reichstein, M., Knohl, A., et al. (2017). Impacts of droughts and extreme temperature events on gross primary production and ecosystem respiration: A systematic assessment across ecosystems and climate zones. *Biogeosciences Discussions*, 1–39. <https://doi.org/10.5194/bg-2017-393>
- Wagle, P., Xiao, X. M., & Suyker, A. E. (2015). Estimation and analysis of gross primary production of soybean under various management practices and drought conditions. *ISPRS Journal of Photogrammetry and Remote Sensing*, *99*, 70–83. <https://doi.org/10.1016/j.isprsjprs.2014.10.009>
- Wagle, P., Zhang, Y. G., Jin, C., & Xiao, X. M. (2016). Comparison of solar-induced chlorophyll fluorescence, light-use efficiency, and process-based GPP models in maize. *Ecological Applications*, *26*(4), 1211–1222. <https://doi.org/10.1890/15-1434>
- Wang, C., Hunt, E. R., Zhang, L., & Guo, H. D. (2013). Phenology-assisted classification of C3 and C4 grasses in the U.S. Great Plains and their climate dependency with MODIS time series. *Remote Sensing of Environment*, *138*, 90–101. <https://doi.org/10.1016/j.rse.2013.07.025>
- Welp, L. R., Randerson, J. T., & Liu, H. P. (2007). The sensitivity of carbon fluxes to spring warming and summer drought depends on plant functional type in boreal forest ecosystems. *Agricultural and Forest Meteorology*, *147*(3–4), 172–185. <https://doi.org/10.1016/j.agrformet.2007.07.010>
- Wolf, S., Eugster, W., Ammann, C., Häni, M., Zielis, S., Hiller, R., et al. (2013). Corrigendum: Contrasting response of grassland versus forest carbon and water fluxes to spring drought in Switzerland. *Environmental Research Letters*, *8*(3), 035007. <https://doi.org/10.1088/1748-9326/8/3/035007>
- Wolf, S., Keenan, T. F., Fisher, J. B., Baldocchi, D. D., Desai, A. R., Richardson, A. D., et al. (2016). Warm spring reduced carbon cycle impact of the 2012 US summer drought. *Proceedings of the National Academy of Sciences of the United States of America*, *113*(21), 5880–5885. <https://doi.org/10.1073/pnas.1519620113>
- Xiao, X. M., Hollinger, D., Aber, J., Goltz, M., Davidson, E. A., Zhang, Q. Y., & Moore, B. (2004). Satellite-based modeling of gross primary production in an evergreen needleleaf forest. *Remote Sensing of Environment*, *89*(4), 519–534. <https://doi.org/10.1016/j.rse.2003.11.008>
- Xiao, X. M., Zhang, Q. Y., Braswell, B., Urbanski, S., Boles, S., Wofsy, S., et al. (2004). Modeling gross primary production of temperate deciduous broadleaf forest using satellite images and climate data. *Remote Sensing of Environment*, *91*(2), 256–270. <https://doi.org/10.1016/j.rse.2004.03.010>
- Xin, Q., Broich, M., Suyker, A. E., Yu, L., & Gong, P. (2015). Multi-scale evaluation of light use efficiency in MODIS gross primary productivity for croplands in the Midwestern United States. *Agricultural and Forest Meteorology*, *201*, 111–119. <https://doi.org/10.1016/j.agrformet.2014.11.004>
- Yuan, W., Cai, W., Chen, Y., Liu, S., Dong, W., Zhang, H., et al. (2016). Severe summer heatwave and drought strongly reduced carbon uptake in southern China. *Scientific Reports*, *6*(1), 18813. <https://doi.org/10.1038/srep18813>
- Yuan, W. P., Cai, W. W., Nguy-Robertson, A. L., Fang, H. J., Suyker, A. E., Chen, Y., et al. (2015). Uncertainty in simulating gross primary production of cropland ecosystem from satellite-based models. *Agricultural and Forest Meteorology*, *207*, 48–57. <https://doi.org/10.1016/j.agrformet.2015.03.016>
- Yuan, W., Cai, W., Xia, J., Chen, J., Liu, S., Dong, W., et al. (2014). Global comparison of light use efficiency models for simulating terrestrial vegetation gross primary production based on the LaThuile database. *Agricultural and Forest Meteorology*, *192–193*, 108–120. <https://doi.org/10.1016/j.agrformet.2014.03.007>
- Zhang, Y., Song, C., Sun, G., Band, L. E., Noormets, A., & Zhang, Q. (2015). Understanding moisture stress on light use efficiency across terrestrial ecosystems based on global flux and remote-sensing data. *Journal of Geophysical Research: Biogeosciences*, *120*, 2053–2066. <https://doi.org/10.1002/2015JG003023>
- Zhang, Y., Xiao, X., Jin, C., Dong, J., Zhou, S., Wagle, P., et al. (2016). Consistency between sun-induced chlorophyll fluorescence and gross primary production of vegetation in North America. *Remote Sensing of Environment*, *183*, 154–169. <https://doi.org/10.1016/j.rse.2016.05.015>
- Zhang, Y., Xiao, X., Wu, X., Zhou, S., Zhang, G., Qin, Y., & Dong, J. (2017). A global moderate resolution dataset of gross primary production of vegetation for 2000–2016. *Scientific Data*, *4*, 170165. <https://doi.org/10.1038/sdata.2017.165>
- Zhang, Y., Xiao, X. M., Zhou, S., Ciais, P., McCarthy, H., & Luo, Y. Q. (2016). Canopy and physiological controls of GPP during drought and heat wave. *Geophysical Research Letters*, *43*(7), 3325–3333. <https://doi.org/10.1002/2016GL068501>
- Zhu, Q., Zhuang, Q., Henze, D., Bowman, K., Chen, M., Liu, Y., et al. (2014). Constraining terrestrial ecosystem CO₂ fluxes by integrating models of biogeochemistry and atmospheric transport and data of surface carbon fluxes and atmospheric CO₂ concentrations. *Atmospheric Chemistry and Physics Discussions*, *14*(16), 22,587–22,638. <https://doi.org/10.5194/acpd-14-22587-2014>
- Zscheischler, J., Mahecha, M. D., von Buttler, J., Harmeling, S., Jung, M., Rammig, A., et al. (2014). A few extreme events dominate global interannual variability in gross primary production. *Environmental Research Letters*, *9*(3), 035001. <https://doi.org/10.1088/1748-9326/1089/1083/035001>